FORUM REVIEW ARTICLE

Nitroxyl Radical as a Theranostic Contrast Agent in Magnetic Resonance Redox Imaging

Ken-ichiro Matsumoto,[1,i] Ikuo Nakanishi,[2] Zhivko Zhelev,[3,4] Rumiana Bakalova,[5] and Ichio Aoki[5]

Abstract

Significance: In vivo assessment of paramagnetic and diamagnetic conversions of nitroxyl radicals based on cyclic redox mechanism can be an index of tissue redox status. The redox mechanism of nitroxyl radicals, which enables their use as a normal tissue-selective radioprotector, is seen as being attractive on planning radiation therapy.
Recent Advances: In vivo redox imaging using nitroxyl radicals as redox-sensitive contrast agents has been developed to assess tissue redox status. Chemical and biological behaviors depending on chemical structures of nitroxyl radical compounds have been understood in detail. Polymer types of nitroxyl radical contrast agents and/or nitroxyl radical-labeled drugs were designed for approaching theranostics.
Critical Issues: Nitroxyl radicals as magnetic resonance imaging (MRI) contrast agents have several advantages compared with those used in electron paramagnetic resonance (EPR) imaging, while support by EPR spectroscopy is important to understand information from MRI. Redox-sensitive paramagnetic contrast agents having a medicinal benefit, that is, nitroxyl-labeled drug, have been developed and proposed.
Future Directions: A development of suitable nitroxyl contrast agent for translational theranostic applications with high reaction specificity and low normal tissue toxicity is under progress. Nitroxyl radicals as redox-sensitive magnetic resonance contrast agents can be a useful tool to detect an abnormal tissue redox status such as disordered oxidative stress. *Antioxid. Redox Signal.* 36, 95–121.

Keywords: theranostics, redox imaging, nitroxyl radical, redox-sensitive contrast agent, magnetic resonance imaging, electron paramagnetic resonance

Introduction

THE TERM "REDOX" is a word created by combining reduction and oxidation. Reduction means receiving an electron and oxidation means losing an electron; therefore, reduction and oxidation, that is, a redox reaction, occur simultaneously. Redox is the exchange of an electron between molecules. All life is maintained by systematically regulated redox reactions. An exogenous compound introduced into a living cell system is reduced or oxidized according to the tissue redox status/balance. The tissue redox status is an index of activity or condition of cells constituting the tissue. A hypoxic environment in cancer/tumor tissue produced by uncontrolled vasculature may shift the redox balance in the

[1]Quantitative RedOx Sensing Group, Department of Radiation Regulatory Science Research, National Institute of Radiological Sciences, Quantum Life and Medical Science Directorate, National Institutes for Quantum and Radiological Science and Technology, Chiba-shi, Japan.
[2]Quantum RedOx Chemistry Group, Institute for Quantum Life Science, Quantum Life and Medical Science Directorate, National Institutes for Quantum and Radiological Science and Technology, Chiba-shi, Japan.
[3]Medical Faculty, Trakia University, Stara Zagora, Bulgaria.
[4]Institute of Biophysics and Biomedical Engineering, Bulgarian Academy of Sciences, Sofia, Bulgaria.
[5]Functional and Molecular Imaging Goup, Department of Molecular Imaging and Theranostics, Institute for Quantum Medical Science, Quantum Life and Medical Science Directorate, National Institutes for Quantum and Radiological Science and Technology, Chiba-shi, Japan.
[i]ORCID ID (https://orcid.org/0000-0002-8151-4067).

tissues/cells (18, 36, 134). Collapsed vasculatures in wound tissue make tissue hypoxic and shift the redox status in tissue (82, 141, 160). Pathological conditions in tissues/cells, such as inflammation, can also alter the tissue redox status (63, 130).

Redox imaging, which can visualize the redox status of a target tissue/organ noninvasively, was developed as a diagnostic technique for analyzing redox physiology, investigating oxidative stress in animal pathophysiological models, and improving radiation therapy. Redox sensing using nitroxyl radicals was initially developed in the field of *in vivo* electron paramagnetic resonance (EPR) spectroscopy (3, 46, 65, 132). The historical development of *in vivo* EPR instruments and techniques was well summarized in previous review articles (10, 169). Nitroxyl radicals are stable free radical species when dry or dissolved in pure water, and they are directly detectable by EPR at room temperature. The nitroxyl radicals are reduced to corresponding hydroxylamines when administered to a living experimental animal (64, 121, 131). The rate constant of this *in vivo* reduction of nitroxyl radicals varies according to oxidative stress (144, 178, 184). An unbalanced tissue redox status, that is, faster or slower reduction rate of nitroxyl reduction beyond a normal range, can be considered an index of failure of redox metabolism in the tissue (102).

Since the early 2000s, nitroxyl radicals have been used as a redox-sensitive contrast agent, which was so-called spin probe at that time, in EPR imaging (EPRI) experiments (99, 104, 180, 189). When combined with EPRI, the distribution and time course of nitroxyl contrast agents in tissues can be observed (118, 123, 166). Although the temporal resolution of EPRI in that time was in the order of minutes due to the magnetic field scans based on continuous wave (CW) modality, the current temporal resolution of CW EPRI has markedly improved (159).

Nitroxyl radical compounds, which have an unpaired electron, are paramagnetic species and exert T_1-shortening effects on nuclear spin similar to gadolinium compounds. Therefore, nitroxyl radical in an aqueous sample can be detected by enhanced T_1-weighted contrast on magnetic resonance imaging (MRI). Mapping of the *in vivo* redox status of a target tissue, such as cancer/tumor, can be achieved by T_1-weighted MRI with nitroxyl radicals as the contrast agent (119). Spatial and temporal high-resolution redox mapping of a particular slice is possible with excellent anatomical information from MRI.

Overhauser-enhanced MRI (OMRI) or proton electron double resonance imaging (PEDRI) is another magnetic resonance technique for imaging nitroxyl radicals *in vivo* (123, 166). These techniques can produce and observe dynamic nuclear polarization (DNP) effect *in vivo* by injecting a nitroxyl radical compound into experimental animals (24, 41, 186). Nitroxyl compounds are not suitable for producing better DNP effects due to the relatively broad EPR line width, that is, fast relaxation time, even using a ^{15}N-labeled nitroxyl radical compound. However, OMRI can observe spectral information based on EPR and high image resolution based on MRI, and therefore this multimodality is advantageous for future theranostic approaches.

In this review, the authors describe the detection and analysis of redox reactions using a stable nitroxyl radical probe *in vitro* and *in vivo*. Recent applications of imaging the tissue redox status using stable nitroxyl radicals as redox-sensitive MRI contrast agents are also discussed. In addition, theranostic approaches and/or translational applications of magnetic resonance (MR) redox imaging techniques are introduced.

Chemistry and Redox Properties of Nitroxyl Radicals

Cyclic nitroxyl radicals with methyl groups at the carbons adjacent to the nitrogen are stable under ambient conditions and exhibit unique redox properties. Recently, their detailed chemical and electrochemical properties were reviewed (105, 106, 142). They (2,2,6,6-tetramethylpiperidine-*N*-oxyl: TEMPO as a representative example) undergo reversible one-electron oxidation reactions to produce the corresponding oxoammonium cations (oxoammonium form of TEMPO [TEMPO$^+$]) (Fig. 1). A reversible cyclic voltammogram was first reported for TEMPO in 1973 (177). The six-membered ring nitroxyl radicals are generally oxidized at lower potentials than the five-membered ring compounds (11, 76, 111). The greater flexibility of the six-membered ring enables the nitrogen center to planarize more easily upon oxidation than the five-membered ring. The electron-donating groups on the ring stabilize the positive charge on the oxoammonium cations, resulting in the negative shift in the oxidation potentials. Furthermore, a significant negative shift in the oxidation potentials of carbamoyl-PROXYL (3-carbamoyl-2,2,5,5-tetramethylpyrrolidine-*N*-oxyl) and TEMPOL (4-hydroxy-2,2,6,6-tetramethylpiperidine-*N*-oxyl or 4-hydroxy-TEMPO) was reported with increasing solvent polarity (111). The stabilization of the oxoammonium cations by the solvent *via* dipolar interaction leads to a negative shift. The effects of the structure of the nitroxyl radicals on the oxidation potentials have been examined, and a good correlation was demonstrated between experimental oxidation potentials and theoretical values estimated by density functional theory calculations (108, 193).
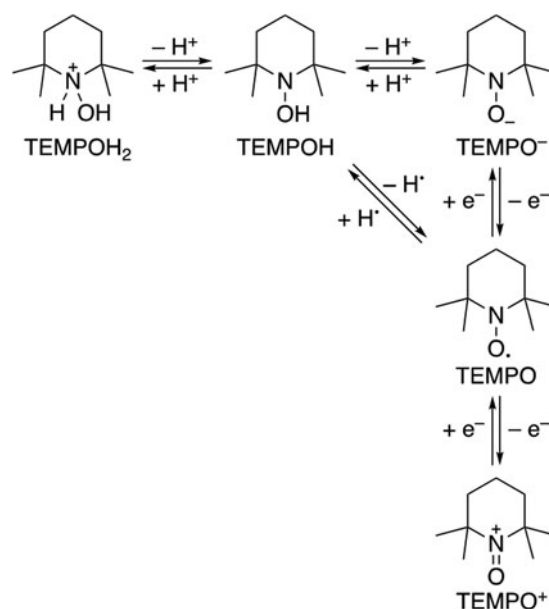

FIG. 1. Redox and acid–base chemistry of TEMPO. TEMPO, 2,2,6,6-tetramethylpiperidine-*N*-oxyl.

Cyclic nitroxyl radicals were reported to undergo chemical oxidation by hydroxyl radicals ($^\bullet$OH), hydroperoxyl radical (HO$_2^\bullet$), RO$_2^\bullet$, $^\bullet$NO$_2$, and CO$_3^{\bullet-}$ (55, 56, 58, 155). The rate constants correlate with their oxidation potentials. The involvement of electron transfer in the reaction of carbamoyl-PROXYL with cumylperoxyl radical was demonstrated by the acceleration in the presence of a redox-inactive metal ion (137), which is known to act as a catalyst in the electron transfer reactions (48, 49).

The reduction processes of the nitroxyl radicals strongly depend on the pH of the solution (89) because they are coupled with proton transfer (Fig. 1). The electrochemical reduction of the cyclic nitroxyl radicals has also been reviewed in detail (105, 106, 142). A marked change in the cyclic voltammograms depending on pH was reported for the reduction of several cyclic nitroxyl radicals (89). Recently, Stahl and colleagues reported a full Pourbaix diagram of TEMPO (Fig. 2), providing valuable information about the pH dependence of its redox properties (52). The reduction potentials of TEMPO shift to the negative direction as the pH of the solution increases, whereas the oxidation potential is pH insensitive.

The 6-membered ring nitroxyl radicals are also reduced at lower potentials than the 5-membered ring radicals due to the flexibility of the ring structure. Furthermore, the substituent effects on the reduction potentials of cyclic nitroxyl radicals were reported (112, 133).

The cyclic nitroxyl radicals are chemically reduced to the corresponding hydroxylamines by biological reductants such as ascorbate (12, 53). Yamada and colleagues demonstrated that the reduction rates of cyclic nitroxyl radicals by ascorbate correlate well with their reduction potentials and Gibbs free energy changes (ΔG) (185). When the ΔG is negative, reduction of the nitroxyl radicals by ascorbate occurs spontaneously, whereas no reduction occurs in the case of a positive ΔG. The involvement of hydrogen tunneling at room temperature was reported based on large kinetic isotope effects (KIE, k_H/k_D) in the reduction of TEMPO by ascorbate in water ($k_H/k_D = 24.2$)

and water–dioxane mixed solvent (1:1 v/v; $k_H/k_D = 31.0$) at room temperature (87, 153). A large KIE of 12.8 was also observed for the reaction of ascorbate with 2-phenyl-4,4,5,5-tetramethylimiazolione-1-oxide (PTIO$^\bullet$) in a phosphate buffer solution at ambient temperatures (138). Thus, quantum tunneling plays a role in the reduction of nitroxyl radicals by ascorbate.

Recently, the catalytic (redox) cycle of TEMPO in the reaction with peroxyl radicals (ROO$^\bullet$) in aqueous solution was proposed by Pratt and colleagues (Fig. 3) (62). TEMPO scavenges ROO$^\bullet$ via electron transfer to produce TEMPO$^+$ and ROO$^-$. Then, a hydride donor, such as NAD(P)H or tetrahydrofuran (THF), converts TEMPO$^+$ to the corresponding hydroxylamine (TEMPO-H). The conversion of TEMPO$^+$ to TEMPO-H by NADH was demonstrated to be via a two-electron transfer reaction (55). TEMPO-H can also scavenge ROO$^\bullet$ via hydrogen-atom transfer to regenerate TEMPO. However, turnover is limited at a low pH due to the protonation of TEMPO-H because the pK_a of TEMPO-H$_2^+$, which is not a hydrogen-atom donor, is 7.34 (Fig. 3). Under hypoxic conditions, the reaction of R$^\bullet$ with oxygen (O$_2$) to produce ROO$^\bullet$ hardly occurs, thus TEMPO is consumed faster by the reaction with R$^\bullet$ to produce TEMPO-R than under aerobic conditions. Furthermore, in the absence of O$_2$, the oxidation of R$^\bullet$ by TEMPO$^+$ takes place to produce R$^+$ and TEMPO (bottom-left dashed arrows in Fig. 3). Under acidic conditions, a comproportionation between TEMPO$^+$ and TEMPO-H occurs to produce two molecules of TEMPO (middle dashed arrow in Fig. 3).

Cyclic nitroxyl radicals were demonstrated to be irreversibly consumed in the presence of thiols (57). The oxidation of thiols by reactive radicals, such as $^\bullet$OH, $^\bullet$NO$_2$, and CO$_3^{\bullet-}$, leads to the corresponding thiyl radicals (RS$^\bullet$). RS$^\bullet$ reacts with the nitroxyl radicals (>NO$^\bullet$) to produce the adduct >NOSR. Under physiological conditions >NOSR is decomposed to the corresponding amine (>NH) (57). These redox conversions are highly informative regarding the chemical reactivity of nitroxyl radicals as in vivo spin probes.
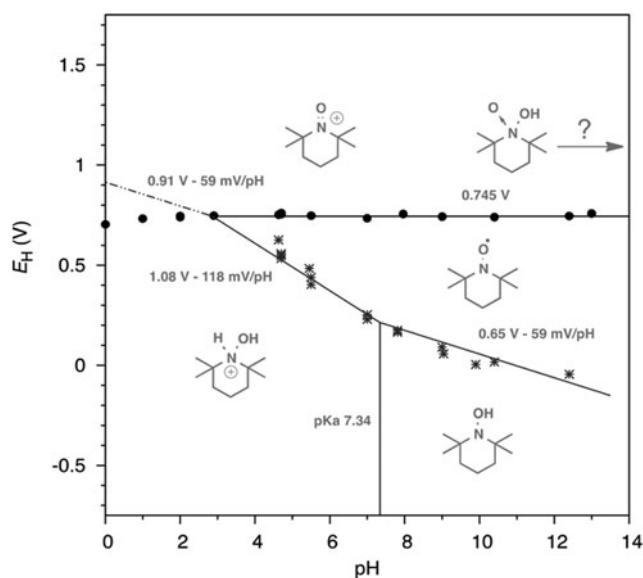

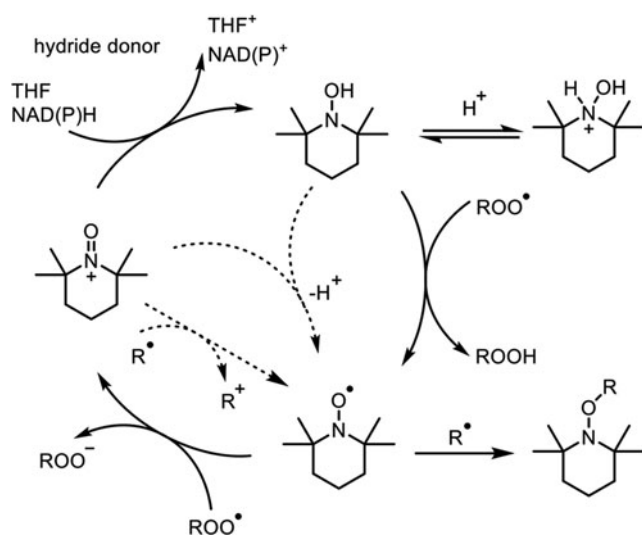**FIG. 2. Pourbaix diagram of TEMPO in buffered aqueous solutions.** [Adapted with permission from Gerken et al. (52). Copyright 2018 American Chemical Society.]

FIG. 3. Redox cycle of TEMPO in the reaction of ROO$^\bullet$. ROO$^\bullet$, peroxyl radical. [Adapted with permission from Griesser et al. (62). Copyright 2018 American Chemical Society.]

Development of Redox Sensing into Redox Imaging

Nitroxyl radicals as a T_1 contrast agent

In the early 1980s, the use of nitroxyl free radicals as T_1 contrast agents in MRI was examined (13). However, nitroxyl radicals were not considered optimal as MR contrast agents due to their low T_1-relaxivity (r_1) and rapid *in vivo* reduction at that time. Current MRI scanners operating with a higher magnetic field, a better signal-to-noise ratio, and efficient pulse sequences make it possible to reconsider nitroxyl radicals as potential T_1 contrast agents.

The indirect detection of nitroxyl radicals based on proton MR T_1 contrast is not quantitative. However, the low r_1 of nitroxyl radicals gives an almost linear relationship between T_1 enhancement and the concentration of a contrast agent in a lower concentration region (117). T_1-weighted images of an identical phantom containing several concentrations of solutions of a nitroxyl radical, MC-PROXYL (3-methoxycarbonyl-2,2,5,5-tetramethylpyrrolidine-*N*-oxyl), scanned with the same fast low angle shot (FLASH) sequence using 1- and 7 T scanners are shown in Figure 4 (135). The r_1 of nitroxyl radicals was estimated to be $0.27\,\mathrm{m}M^{-1}\cdot\mathrm{s}^{-1}$ at 1 T and $0.14\,\mathrm{m}M^{-1}\cdot\mathrm{s}^{-1}$ at 7 T, and good linearity was observed for the relationship between T_1 enhancement and the concentration when the concentration was <3 mM. A plot of simulated values of T_1-weighted gradient echo MR contrast *versus* the concentration of nitroxyl radicals calculated using a r_1 of $0.14\,\mathrm{m}M^{-1}\cdot\mathrm{s}^{-1}$ is shown in Figure 5. The simulation revealed an almost linear relationship between percentage signal amplification of T_1-weighted image (ΔM%) and the concentration of nitroxyl contrast agent with an $R^2 = 0.9991$ when the concentration range was <3 mM (Fig. 5C). Although the decay rate of ΔM% was slightly different from the true reduction rate of nitroxyl radicals, the differences were sufficiently small when parameters in practical ranges were used (117).

Loading decay rate of nitroxyl radicals on the image

By attaching an additional dimension to a simple distribution image, we can obtain functional information from a set of images. The time axis is easily attached by sequential measurement of several images (118, 123). Consequently, EPR signal decay rates calculated in a pixel-wise manner, namely decay rate mapping, can be obtained.

Evidence of a faster decay rate of nitroxyl radicals in tumor tissues was obtained from EPRI experiments (101, 166). A nitroxyl radical called carbamoyl-PROXYL decayed faster in a RIF-1 tumor than in the normal tissue (101). Another study also reported that carbamoyl-PROXYL decayed faster in a SCCVII tumor than in the normal tissue (166).

The MR signal is composed of the intrinsic signal of the tissue and enhancement with nitroxyl contrast agent. To calculate the contribution of nitroxyl radicals to the enhanced T_1-weighted MR signal, the baseline signal, that is, intrinsic T_1-weighted signal of tissue before the administration of contrast agent, must be subtracted from that after the administration of contrast agent (Fig. 6). The MR signal was composed of tissue T_1 and nitroxyl radical-induced T_1 signals.

The time course of chemical reduction of a nitroxyl radical using ascorbate was compared by EPRI and T_1-weighted MRI (Fig. 7) (119). MRI yields a higher spatial and temporal resolution than EPRI, but the resulting decay rates are
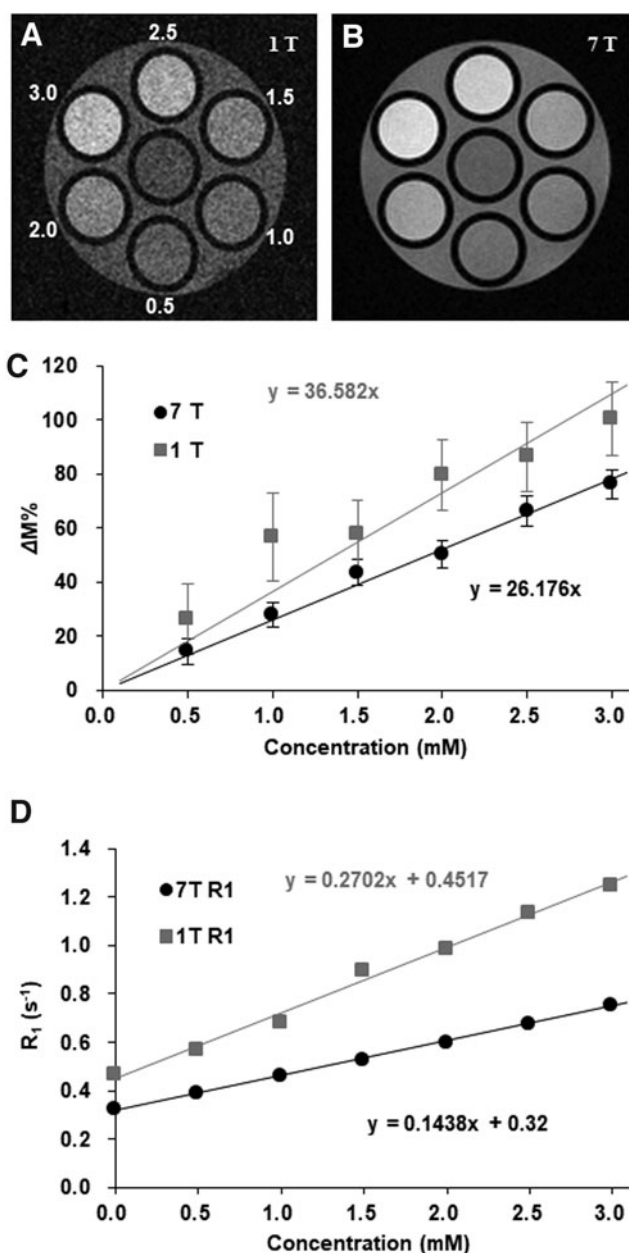

FIG. 4. A comparison of percentage signal amplification of T_1-weighted image (ΔM%) and T_1-relaxivity (r_1) of a nitroxyl radical, MC-PROXYL, between different magnetic fields 1 and 7 T. An identical 7-tube phantom was scanned by FLASH (TE = 5.1 ms, TR = 75 ms, FA = 45°), and T_1-weighted images at **(A)** 1 T and **(B)** 7 T were obtained. The *number* indicated in **(A)** is the concentration of MC-PROXYL. The *center* tube contains water. **(C)** Relationships of ΔM% and concentrations of MC-PROXYL were almost linear. **(D)** T_1 relaxation rates (R_1) observed from T_1 mapping of the phantom were plotted *versus* the corresponding concentration of MC-PROXYL, and r_1 was obtained from slopes of the plots as $0.27\,\mathrm{m}M^{-1}\cdot\mathrm{s}^{-1}$ for 1 T and $0.14\,\mathrm{m}M^{-1}\cdot\mathrm{s}^{-1}$ for 7 T. FA, flip angle; FLASH, fast low angle shot; MC-PROXYL, 3-methoxycarbonyl-2,2,5,5-tetramethylpyrrolidine-*N*-oxyl; TE, echo time; TR, repetition time. The figure was partly modified from our previous report (135).
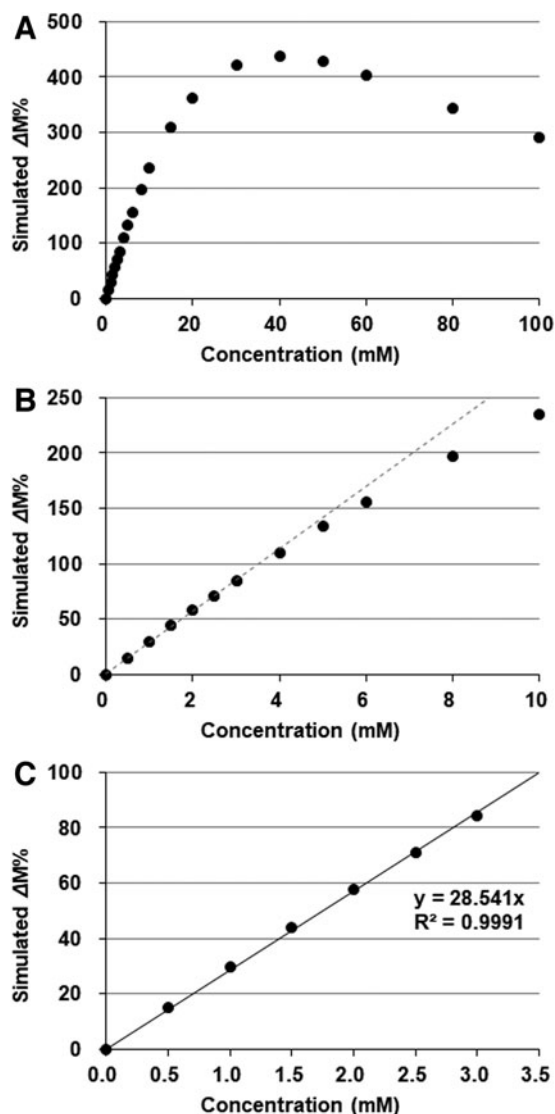
FIG. 5. Relationship between the concentration of nitroxyl contrast agent and simulated $\Delta M\%$ of T_1-weighted image. (A) $\Delta M\%$ increased with the concentration of paramagnetic nitroxyl contrast agent, then peaked and decreased. (B) The relationship between $\Delta M\%$ and concentration of nitroxyl contrast agent slightly curved at the lower concentration region $<10\,mM$. (C) Fairly good linearity ($R^2 = 0.9991$) was obtained between the simulated $\Delta M\%$ and concentration of nitroxyl contrast agent for the concentration region $<3\,mM$. Values used for the simulation were as follows: $r_1 = 0.14\,mM^{-1}\cdot s^{-1}$, $M_0 = 1000$, $TR = 75\,ms$, $TE = 5.1\,ms$, $FA = 45°$, T_1 of water $= 2350\,ms$, and $T_2^* = 50\,ms$.

similar. The decay rate obtained from MR T_1 contrast can be handled as a proxy-decay rate, which is not the same as the original EPR decay rate, but the theoretical error between the proxy- and original EPR decay rates is sufficiently small under biological conditions (117).

Advantages of MR detection of nitroxyl contrast agents

A relatively broad EPR linewidth and hyperfine splitting make the EPR signal intensity low in EPRI. The signal/noise ratio of EPR images decreases depending on the complica-
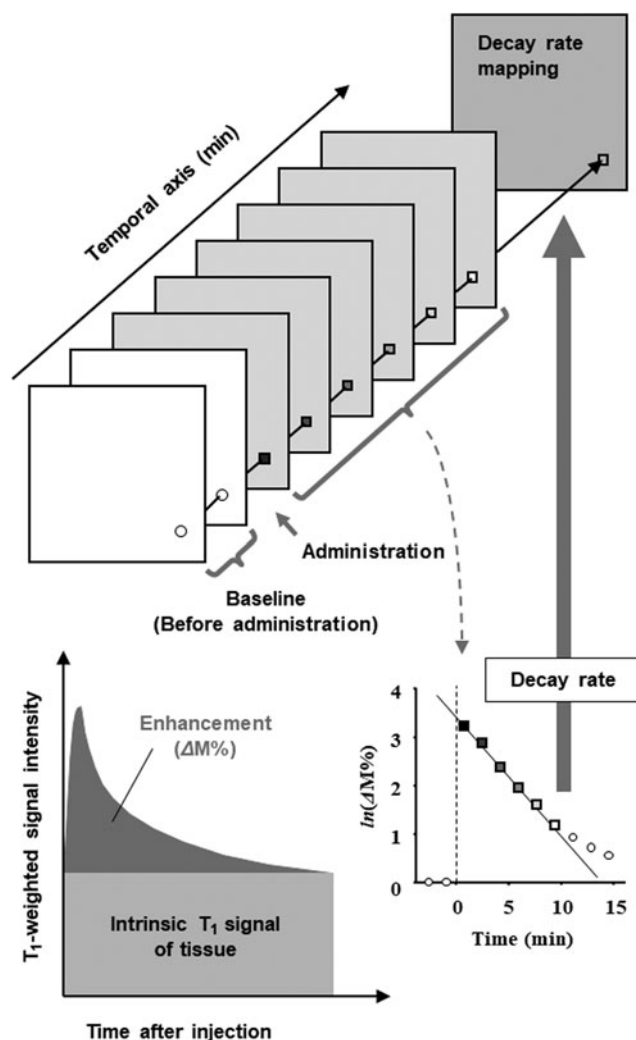

FIG. 6. A schematic drawing of the concept of MR redox imaging. The additional time dimension to the 2D or 3D mapping of the contrast agent can provide functional information such as pharmacokinetics of the nitroxyl radical. The time axis can be provided by repeated scanning of an identical ROI. The $\Delta M\%$ of the T_1-weighted image, which is the contribution of T_1 enhancement by nitroxyl radicals, was obtained by subtracting the baseline image from those observed after administration of the contrast agent. As a result, pixel-wise decay rates of nitroxyl radicals can be obtained. 2D, two dimensional; 3D, three dimensional; MR, magnetic resonance; ROI, region of interest.

tion of hfs and linewidth (anisotropy) even if deconvolution techniques are used to remove spectral information (123). T_1-weighted MRI can simplify the detection of nitroxyl contrast agents. This may be a great advantage to modify nitroxyl contrast agents chemically and to design organ/tissue specificity for *in vivo* use. The lower quantification ability of T_1-weighted MRI may not be problematic for redox estimation. Detection of nitroxyl by T_1-weighted MRI is fast and provides high resolution.

Coupling multiple nitroxyl molecules can improve the T_1-weighted contrast effects of nitroxyl-based contrast agents (124). A good linear relationship was obtained between T_1-weighted image enhancement and the concentration of the

contrast agent up to three spins in a molecule. The r_1 levels of nitroxyl contrast agents increase depending on the number of nitroxyl spins in a molecule. Although the coupling of multiple nitroxyl molecules broadens its EPR spectrum and makes EPRI difficult, T_1-weighted MRI techniques enable the mapping of the multispin nitroxyl contrast agents. However, support by EPR spectroscopy remains important to understand information from MRI.

Mapping the *in vivo* nitroxyl decay rate in a SCCVII tumor on the mouse thigh was measured using MRI (119). The location of the axial slices including the SCCVII tumor and normal leg of a mouse is shown in Figure 8A. T_1 contrast was enhanced in both normal and tumor tissues after the administration of carbamoyl-PROXYL, and then it gradually decreased (Fig. 8B). The time course of T_1 contrast in the region of interest (ROI)-1 and ROI-2 is shown in Figure 8C. The tumor region exhibited a faster decay rate than the normal region. The decay rate mapping (Fig. 8D) demonstrated a notable difference in decay rates between tumor tissue and the normal tissue. The difference between tumor tissue and normal tissue remained around the tumor tissues and was clear due to the high spatial resolution.

Redox information rather than clearance

Hydroxylamine can be easily oxidized to the corresponding nitroxyl radical by adding a strong oxidant such as potassium ferricyanide. Then, the total amount of contrast agent in the tissue, including the nitroxyl radical form plus hydroxylamine form, can be measured by EPR. The time course of the total amount of contrast agent in both the tumor and normal tissues was stable during the time period used in the imaging experiment (Fig. 9). Therefore, the *in vivo* disappearance of EPR signal and T_1 contrast induced by a nitroxyl contrast agent is due to reduction (119).

FIG. 7. A comparison of chemical reduction courses of a nitroxyl radical monitored by EPRI or T_1-weighted spoiled gradient echo MRI. (*Upper panel*) A phantom used for experiments. (*Left column* of *lower panel*) A time course of EPR images and the signal decay profile in the ROI. (*Right column* of *lower panel*) A time course of ΔM% signal of T_1-weighted MRI and the signal decay profile in the ROI. An identical cylindrical phantom (internal diameter, 1.27 cm) was set in the 30×50 mm (diameter $\times$ length) Litz resonator operating at 300 MHz EPR or a birdcage-type MRI coil. The cylinder was previously filled with 50 mM phosphate buffer (pH 7.4). The same volume of 4 mM carbamoyl-PROXYL solution and 10 mM AA solution was simultaneously delivered into the cylinder with the same flow rate using a stopped-flow system; then the flow was stopped after the internal volume of the cylinder was replaced by the reaction mixture. Scans were started 5 min before the starting reaction and repeated at 2.3-min intervals for EPRI and 30-s interval for MRI. The signal decay rates were obtained from the slope of the linear portion of the decay curves. AA, ascorbic acid; carbamoyl-PROXYL, 3-carbamoyl-2,2,5,5-tetramethylpyrrolidine-N-oxyl; EPR, electron paramagnetic resonance; EPRI, EPR imaging; MRI, magnetic resonance imaging. The figure was partly modified from our previous report (119).

The pharmacokinetics of three different nitroxyl contrast agents with different membrane permeability were investigated (79). TEMPOL is an amphiphilic molecule with high membrane permeability. Carbamoyl-PROXYL has slight membrane permeability. However, carboxy-PROXYL (3-carboxy-2,2,5,5-tetramethylpyrrolidine-N-oxyl) is membrane impermeable. T_1-weighted signal amplification (ΔM%) images and pharmacokinetic profiles after the administration of nitroxyl contrast agents are shown in Figure 10. The concentration of the free radical forms of nitroxyl contrast agents in the tissue calculated based on the enhancement of T_1 contrast and the concentration of the total amount of contrast agents according to EPR measurement were compared (Fig. 10, lower panels). For TEMPOL and carbamoyl-PROXYL, T_1 contrast decay curves demonstrated faster decay than that of the total contrast agents. Carboxy-PROXYL, however, exhibited similar decay slopes between T_1 contrast and the total contrast agent. Cell-impermeable nitroxyl radicals are stable against reduction. Redox imaging
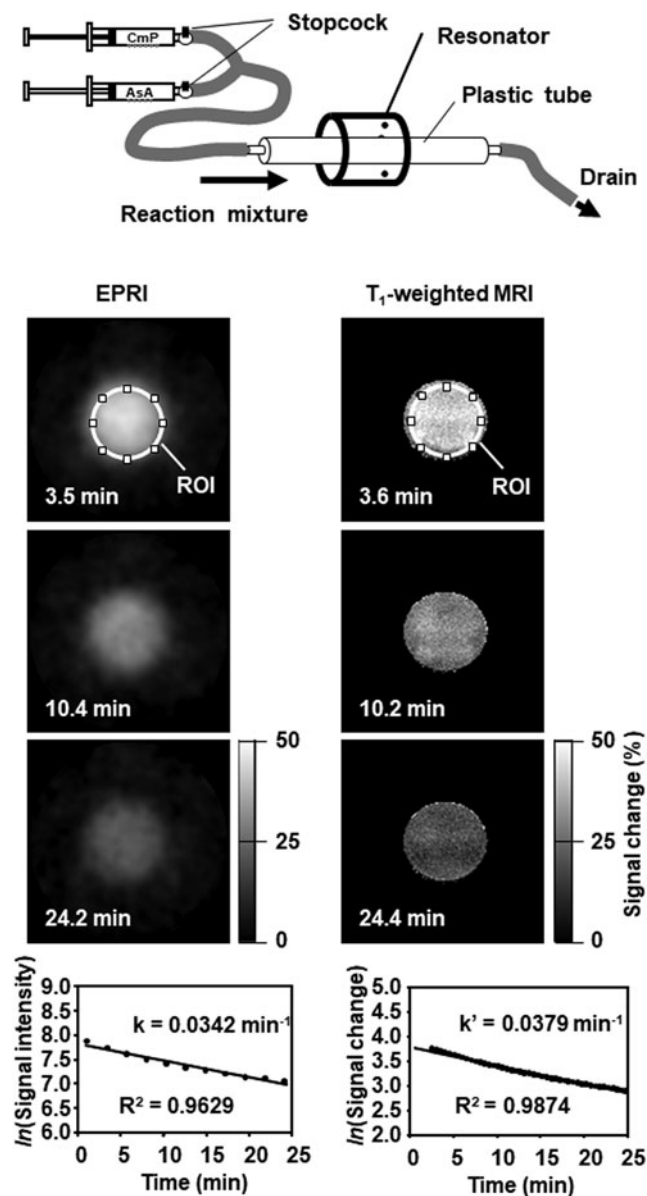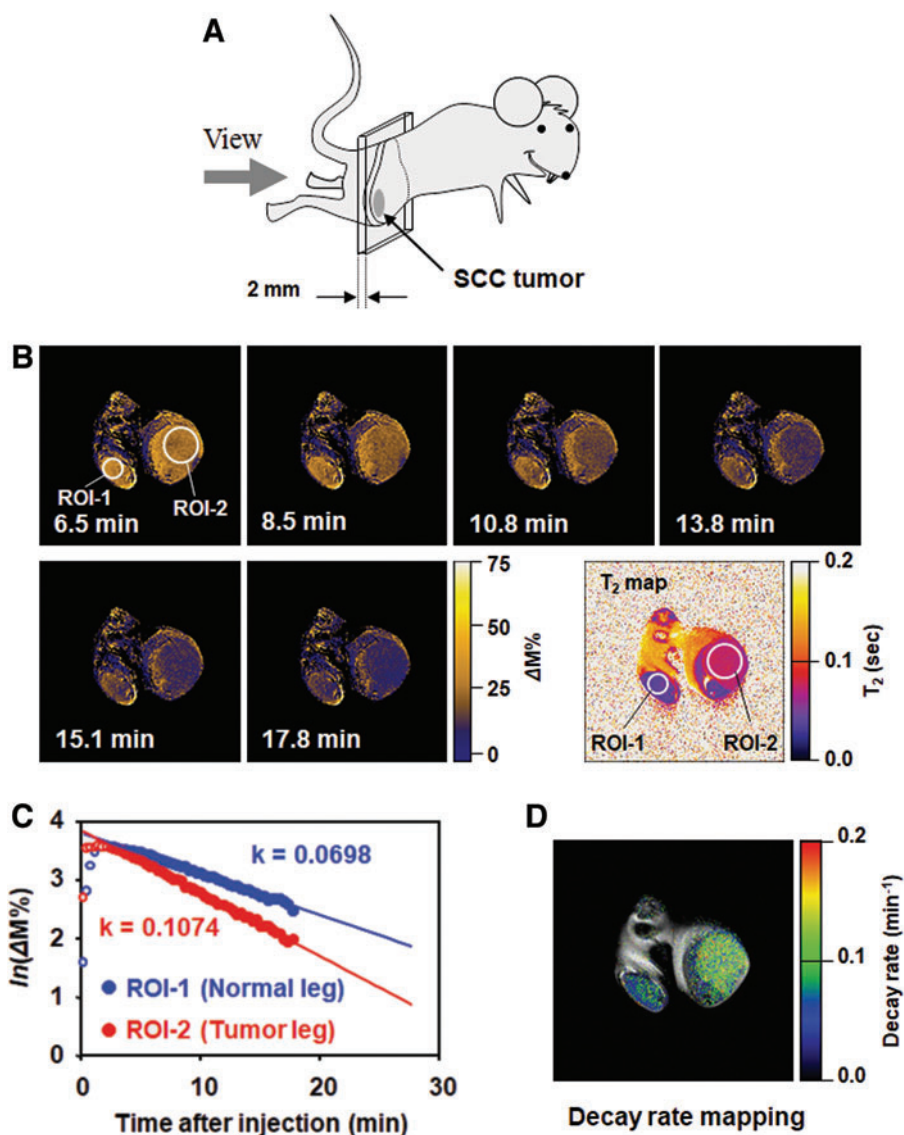
FIG. 8. An example of MR-based redox imaging. (A) Direction of the slice view of MRI with respect to the subject mouse. **(B)** Time course of $\Delta M\%$ signal of T_1-weighted MRI and scout T_2 mapping for ROI selection. Time after injection is indicated in each image. ROI-1 for normal leg and ROI-2 for tumor leg were estimated based on previous T_2 mapping. The field of view was 3.2×3.2 cm. **(C)** Time course of average $\Delta M\%$ signal in ROI-1 and ROI-2. Logarithmic values of $\Delta M\%$ signal in the ROIs are plotted against time. Decay rate constants were obtained from the slope of linear decay after the peak. **(D)** The decay rate map overlapped on the corresponding multislice multiecho image shows the distribution of decay rates with clear anatomic information. The figure was partly modified from our previous report (119). Color images are available online.

techniques using a combination of a membrane-permeable nitroxyl radical and dynamic scanning T_1-weighted MRI can provide redox information for the target tissue.

Approaches of redox imaging to planning radiation therapy

Ionizing radiation ionizes or excites water molecules, and then generates $^\bullet$OH, hydrogen radicals ($^\bullet$H), hydrated electrons (e^-_{aq}), and other ions (129). Due to its markedly high reactivity, $^\bullet$OH is generally considered to be the major oxidative attacker in radiation biology. Molecular O_2 can react with $^\bullet$H to make a $HO_2^\bullet$ and superoxide ($O_2^{\bullet-}$). Hydrogen peroxide (H_2O_2) can be generated by the reaction of $2\ HO_2^\bullet$ or reaction of $2\ ^\bullet$OH. As 70%–80% of the body volume is composed of water molecules, 70%–80% of the effects of ionizing radiation are due to indirect actions, in which directly generated reactive species by water radiolysis or secondary generated species attack biological molecules. Therefore, most of the effects of radiation are due to the oxidative stress by such reactive oxygen species (ROS).

The results of radiation therapy would be affected by physiological and/or pathological conditions in the target tissues, especially by the low partial oxygen pressure (pO_2) in cancer/tumor tissues. The tissue pO_2 affects the yield of secondary ROS such as H_2O_2, $O_2^{\bullet-}$, and/or other reactive species in the tissue (122). Therefore, the tissue pO_2 and/or accompanying tissue redox status is important for the effectiveness of radiation therapy. For safer and more accurate cancer/tumor radiation therapy, a diagnostic method for tissue pO_2 and/or tissue redox status using a noninvasive functional imaging technique is required (123, 166).

The time course of redox status in the mouse brain after irradiation by X-rays or carbon-ion-beams was investigated (136). The signal decay rate k_1 decreased several hours after irradiation, and then gradually recovered to the original level after X-ray irradiation; however, it mostly recovered or exceeded the original level 1 day after carbon-beam irradiation (Fig. 11). The decrease in k_1 observed several hours after irradiation may be due to reduced blood flow because both decay rates at the later time window k_2, which reflects clearance rather than reduction of nitroxyl radicals, and maximum signal
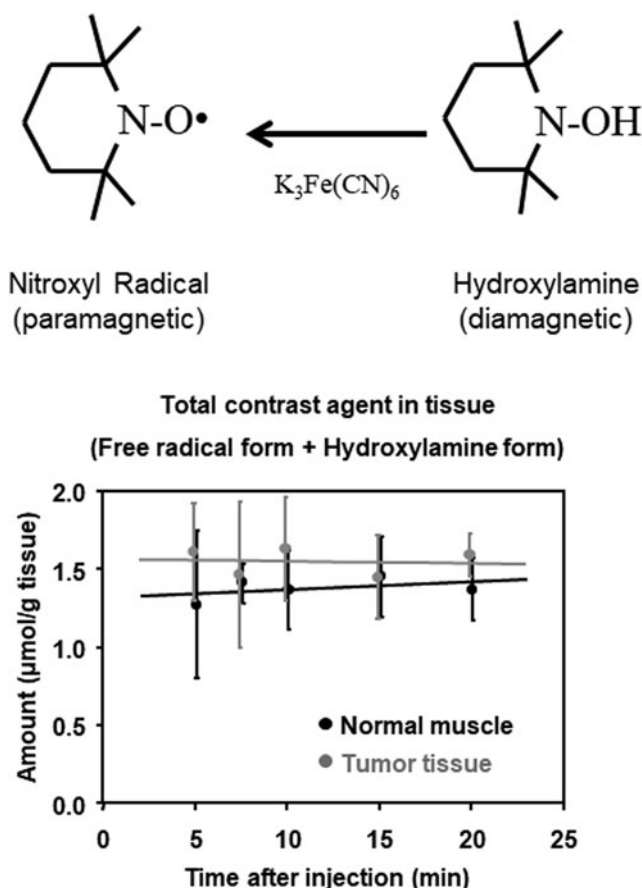
FIG. 9. Time course of total (nitroxyl radical form+hydroxylamine form) amount of carbamoyl-PROXYL in the normal muscle (*black circle*) and tumor tissues (*gray circle*) after the i.v. injection of the nitroxyl radical form of carbamoyl-PROXYL. Each tissue from each mouse was homogenized, and then $K_3[Fe(CN)_6]$ was added to the homogenate to make the final concentration $2\,mM$ for oxidizing the hydroxylamine form to the nitroxyl radical form. The homogenate from each mouse was measured by X-band EPR in triplicate. Marks and error bar indicate the average±SD of three mice. The *horizontal lines* in the figure are obtained by least-squares fitting for the values of normal and tumor tissues. SD, standard deviation. The figure was partly modified from our previous report (119).

intensity temporally decreased several hours after irradiation. The brain exhibited different responses to X-rays and carbon beams. Ionizing radiation can affect the brain tissue redox status for a week, and redox imaging can visualize the tissue status that was not visually discernable.

The biological effects of radiation persist, causing symptoms at a late stage even if there were no visible symptoms at an early stage after irradiation. The prognosis and prevention of late-onset disorders of radiation can be investigated using redox imaging.

Approaches of MR redox imaging for theranostic applications

The mechanism of the radioprotection effects of TEMPOL on the salivary gland was analyzed using MR redox imaging (20). A SCCVII tumor was prepared on the right front leg of

mice to obtain the salivary gland and tumor tissue in an identical slice (Fig. 12A). Increased T_1-weighted MR signal induced by TEMPOL quickly appeared and peaked at 1 min, and then gradually disappeared (Fig. 12B). Natural logarithmic values of TEMPOL-mediated MR intensity in normal muscle, tumor, and salivary gland were plotted as a function of time after the injection of TEMPOL, and then decay rates were obtained from the slopes (Fig. 12C). The decay rate in MR intensity was similar for normal leg tissue and the salivary gland; however, the decay rate was significantly faster in the tumor (Fig. 12D). The differential radioprotection by TEMPOL resides in the faster reduction to the nonradioprotective hydroxylamine in the tumor than in normal tissues.

The hypoxic environment in tumor tissues inhibits reoxidation of a hydroxylamine to the corresponding nitroxyl radical, and the apparent reduction rate consequently markedly increases. Hyodo *et al.* (78) reported that the reduction rate of a nitroxyl radical increased as a function of tumor size (Fig. 13). The markedly higher reduction rates of nitroxyl contrast agents in tumors than in normal tissues can be exploited for diagnosis.

Different redox environment between normal and tumor tissues causes the difference in concentration of nitroxyl radicals between normal and tumor tissues after administration. The concentration of the free radical form in the tumor tissue rapidly decreases and remains around zero; however, that in the normal tissue remains slightly higher due to reoxidation of the hydroxylamine form. The nitroxyl contrast agents can be normal tissue-selective radioprotectors in radiation therapy, which may be carried out after the diagnosis. The nitroxyl contrast agents can be used twice during radiation therapy, first as a redox probe and second as a radioprotector for normal tissues.

Another future possibility of nitroxyl contrast agents is in brain imaging (23, 118, 125). There are several nitroxyl radicals with the ability to permeate the cell membrane because their membrane permeability can be easily regulated by altering a part of the molecule. Nitroxyl-induced T_1 contrast in the mouse head is shown in Figure 14. Different distributions of nitroxyl contrast agents in the brain are observed depending on blood–brain barrier (BBB) permeability. Membrane-impermeable carboxy-PROXYL resulted in no T_1 contrast in the brain (Fig. 14A), whereas carbamoyl-PROXYL, which has slight membrane permeability, partly induced T_1 contrast in the brain (Fig. 14B). Highly permeable MC-PROXYL, 23c [4-(N-methylpiperidine)-2,2,5,5-tetramethylpyrroline-N-oxyl] (23), and TEMPOL demonstrated high T_1 contrast induction in the entire brain (Fig. 14C, E, F). CxP-Am (acetoxymethyl-2,2,5,5-tetramethyl-pyrrolidine-N-oxyl-3-carboxylate), which is a BBB-permeable molecule, was hydrolyzed to membrane-impermeable carboxy-PROXYL in the brain and remained there for a long time (Fig. 14D) (157). The structures of BBB-permeable nitroxyl probes are shown in Supplementary Figure S1.

Investigations of *in situ* or *in vivo* drug delivery using nitroxyl-labeled drugs have long been conducted in the field of EPRI (39, 40, 45). In MRI, Zhelev *et al.* (196) successfully visualized that i.v.-injected TEMPO-labeled nitrosourea (SLENU), which is an anticancer drug labeled by a nitroxyl radical, could penetrate through BBB and distribute into whole brain. This is to say a redox-sensitive paramagnetic contrast agent has a medicinal benefit and vice versa. Using such a hybrid contrast agent, the distribution of the drug and additionally tissue redox status could be observed.
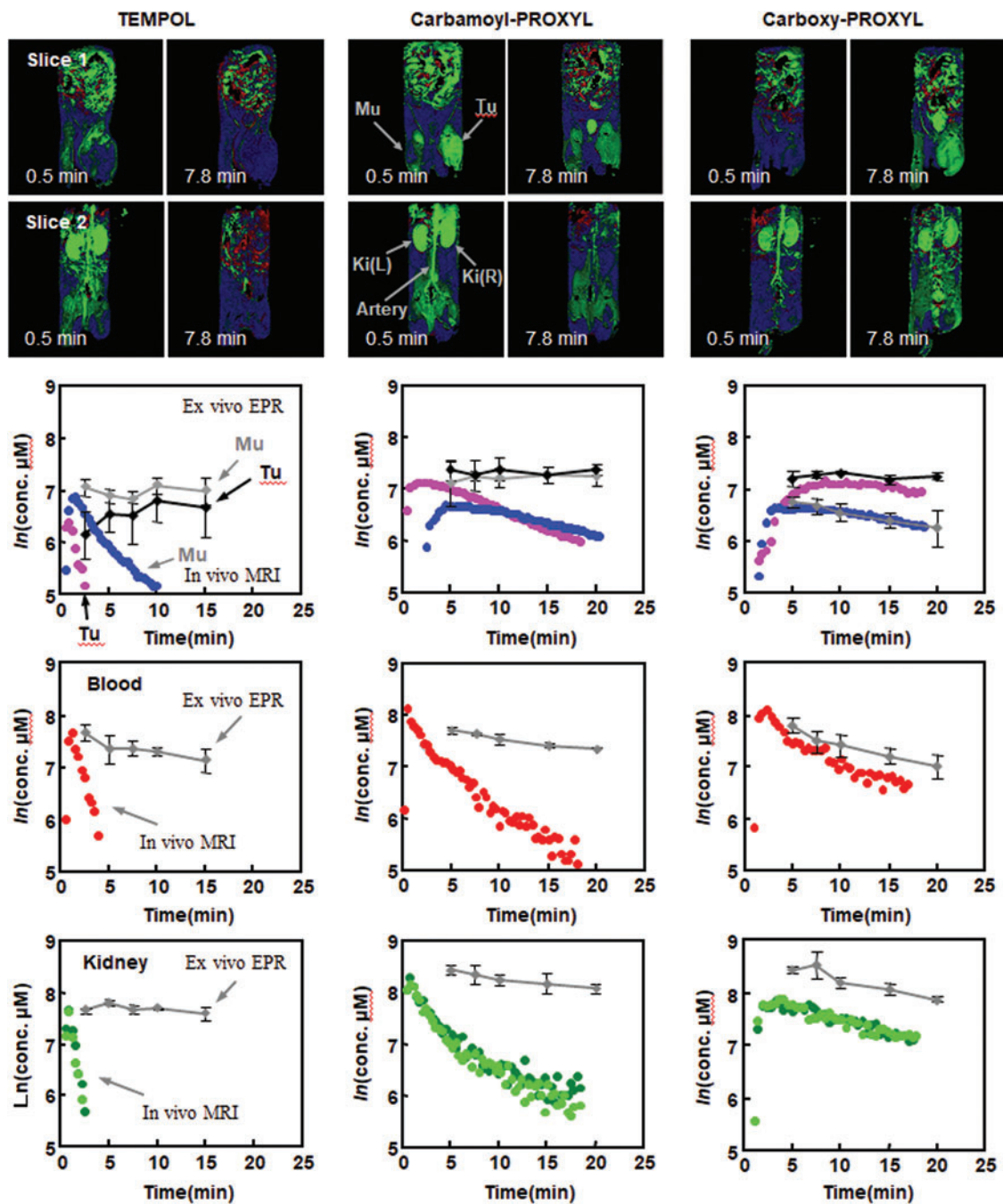
FIG. 10. Comparison of pharmacokinetic profiles of three nitroxyl contrast agents by T_1-weighted MRI. (*Upper image panels*, Slice 1) ΔM% images of a 2 mm-thick slice containing the normal left leg (Mu) and tumor planted on the right leg (Tu) scanned after the administration of TEMOPL (*left*), carbamoyl-PROXYL (*center*), or carboxy-PROXYL (*right*). The time after injection is indicated in each image. (*Lower image panels*, Slice 2) ΔM% images of a 2 mm-thick slice containing the artery and the right and left kidneys, Ki(R) and Ki(L) simultaneously obtained for the same mouse in Slice 1. (*Lower panels*) The pharmacokinetic profiles of the oxidized form and total (nitroxyl radical form+hydroxylamine form) TEMPOL (*left*), carbamoyl-PROXYL (*center*), and carboxy-PROXYL (*right*). The time course of nitroxyl radical form in normal tissue (*blue circle*), tumor tissue (*purple circle*), blood (*red circle*), and kidney (left kidney, *dark green circle*; right kidney, *light green circle*) were obtained by T_1-weighted MRI. The concentrations of total nitroxyl contrast agent (nitroxyl radical+hydroxylamine) measured by X-band EPR spectroscopy in the corresponding tissues are indicated by *gray diamonds* or *black diamonds* for tumor tissue. carboxy-PROXYL, 3-carboxy-2,2,5,5-tetramethylpyrrolidine-*N*-oxyl; TEMPOL, 4-hydroxy-2,2,6,6-tetramethylpiperidine-*N*-oxyl. The figure was partly modified from our previous report (79). Color images are available online.
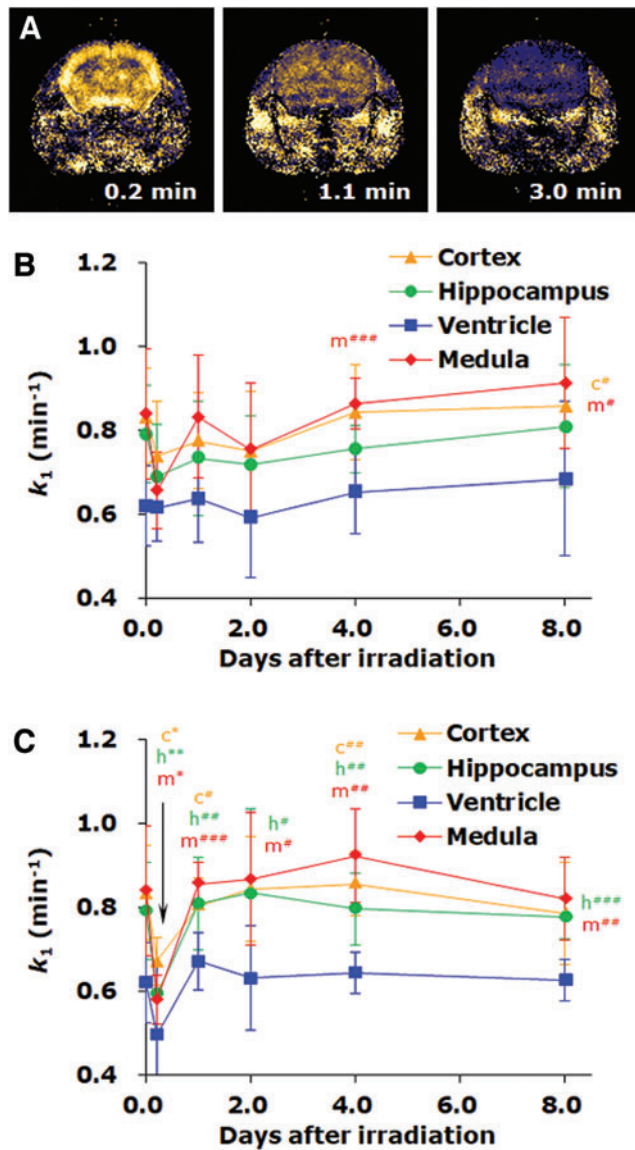
FIG. 11. The time course of redox status in the mouse brain after irradiation by X-rays or carbon-ion-beams. (A) Distribution of a nitroxyl contrast agent, MC-PROXYL, in mouse brain and the time course of $\Delta M\%$. (B) Responses of the k_1 decay rate of MC-PROXYL in the mouse brain after 8 Gy X-ray irradiation for a week. (C) Responses of pharmacokinetic parameters of MC-PROXYL in the mouse brain after 8-Gy carbon-ion-beam irradiation (290 MeV mono beam, LET = 60 keV/μm at the surface) for a week. The values on the *y*-axis (0 day) indicate those for normal healthy mice ($n = 12$). Other values are indicated by the average $\pm$ SD of nine mice for X-rays and of six mice for carbon ion beams, except for the values several hours (0.2 day) after irradiation, which were averaged from three mice. The figure was partly modified from our previous report (136). The letters indicate the initial character of corresponding brain region, and single, double, and triple asterisk(s) or #(s) indicate grades of significance, i.e. $p < 0.05$, $p < 0.01$, and $p < 0.001$, respectively. Color images are available online.
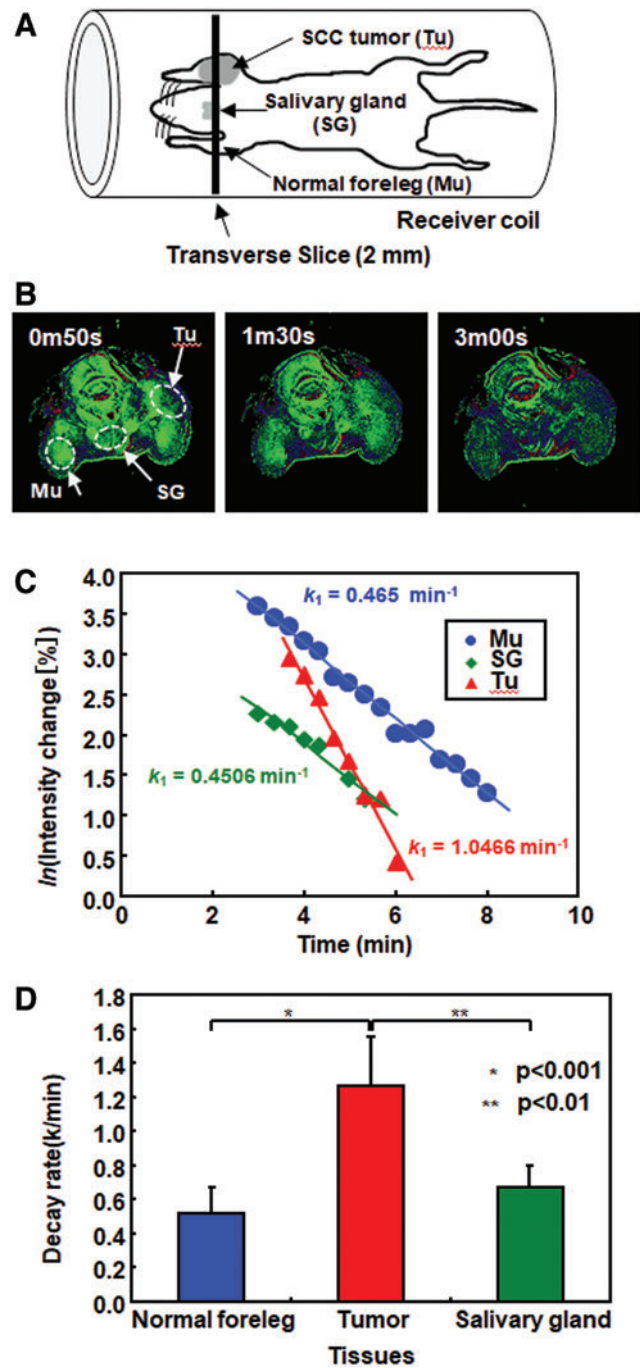

FIG. 12. Comparison of decay rates of TEMPOL in tumor and normal tissues. (A) A schematic drawing of the position of the mouse in the resonator and the slice selected for MRI experiments. A transverse slice (2 mm) covering the normal muscle tissue on foreleg (Mu), SG, and the tumor in the contralateral leg (Tu) was selected to monitor the time course of TEMPOL-induced signal. (B) T_1-weighted images of the selected region after i.v. injection of TEMPOL. The ROIs were selected in the normal leg, SG, and tumor to monitor TEMPOL decay rates. (C) Representative TEMPOL decay profiles after i.v. injection in a mouse for the selected ROIs. (D) Summary of decay rates from the three ROIs in normal muscle, SG, and tumor ($n = 4$ for SG and $n = 6$ for tumor per normal leg). The figure was partly modified from our previous report (20). Color images are available online.
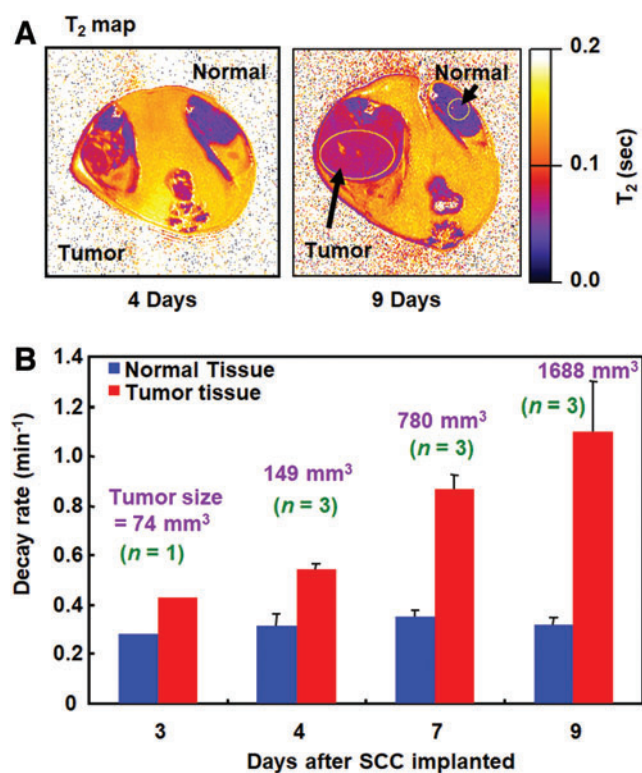
FIG. 13. **Relationship between TEMPOL reduction rate and tumor size. (A)** T_2 map of the SCCVII tumor grown on the hind leg of the same mouse scanned at days 4 and 9. **(B)** Decay rates of TEMPOL in normal muscle and tumor, and the tumor size as a function of time. The figure presents data from experiments in our previous report (78). Color images are available online.

In addition, nitroxyl radicals itself have preventive effects against inflammation, and the mechanisms and applications have been investigated. Deguchi *et al.* (24) reported preventive effects of nitroxyl radical compounds against indomethacin-induced gastric ulcers in rats based on OMRI signal decay. Eguchi *et al.* (37) reported that daily gavage of polymeric micelles possessing nitroxyl radicals for 4 weeks decreases hepatic inflammation in nonalcoholic steatohepatitis model mice. Diagnostic processes of redox status in an inflammatory tissue by a redox imaging with a suitable nitroxyl contrast agent may also be a therapeutic process.

Another design of nitroxyl radical-labeled polymer-type contrast agents, which have dendrimer core and lapping polyethylene glycol chains, was proposed for MRI (139). A nitroxyl radical, fluorophore, prodrug was loaded onto the lapping polymer, and the polymers were conjugated on the core. This structured polymer contrast agent simultaneously works as a drug carrier.

Nitroxyl Radical Contrast Agent for Imaging Redox Imbalance and Oxidative Stress in Living Biological Subjects

Imaging redox imbalance and oxidative stress in the brain

Due to its complex structure and functions, brain is one of the major targets for redox imaging using nitroxyl-enhanced EPRI and MRI, especially at aging, immobilization stress, neurodegenerative damage, hypoxia, and others (156, 179).
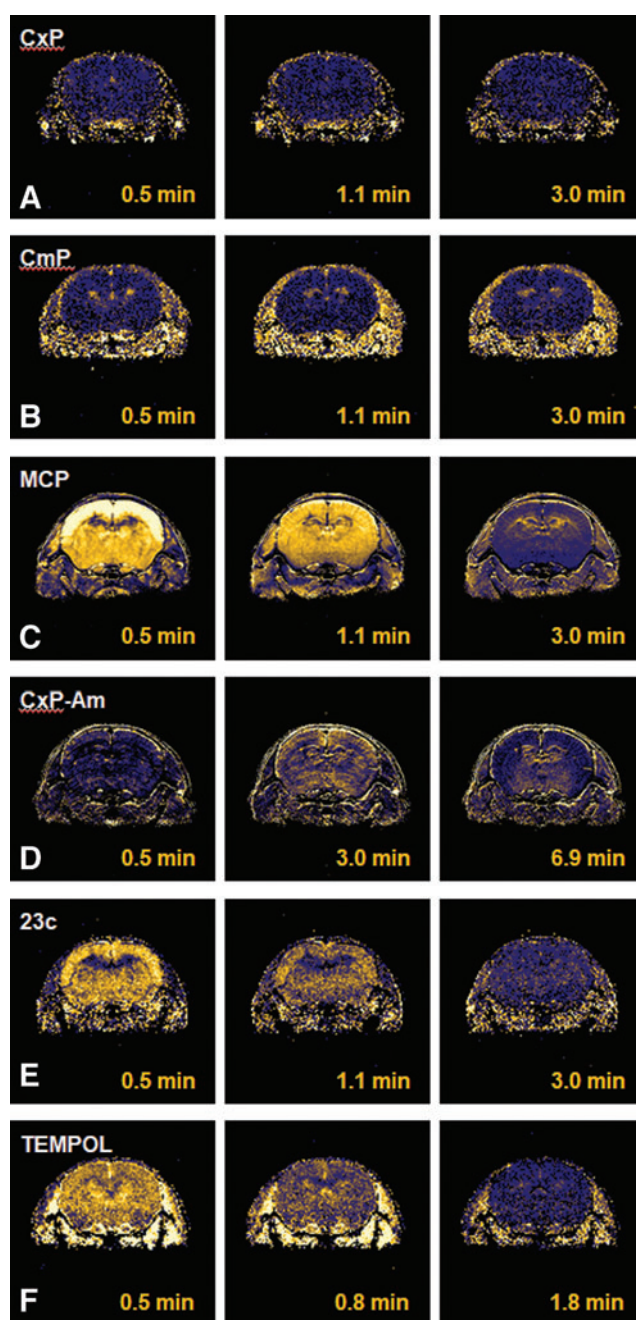
FIG. 14. **Distributions of nitroxyl contrast agents in the mouse brain.** T_1-weighted signal enhancement in the mouse head was observed after i.v. injection of **(A)** carboxy-PROXYL, **(B)** carbamoyl-PROXYL, **(C)** MC-PROXYL, **(D)** CxP-Am, **(E)** 23c, or **(F)** TEMPOL. The *horizontal row* shows the time course of the T_1-weighted signal enhancement. 23c, 4-(*N*-methylpiperidine)-2,2,5,5-tetramethylpyrroline-*N*-oxyl; CxP-Am, acetoxymethyl-2,2,5,5-tetramethyl-pyrrolidine-*N*-oxyl-3-carboxylate. The figure was partly modified from our previous report (125) with some additional data. Color images are available online.

Yokoyama *et al.* published a series of studies on EPRI of brain injuries induced in experimental animals accompanied by the development of oxidative stress (187–191). The authors' basic concept of time-resolved EPRI of the brain is presented in Figure 15 (190). In the brains of rats with

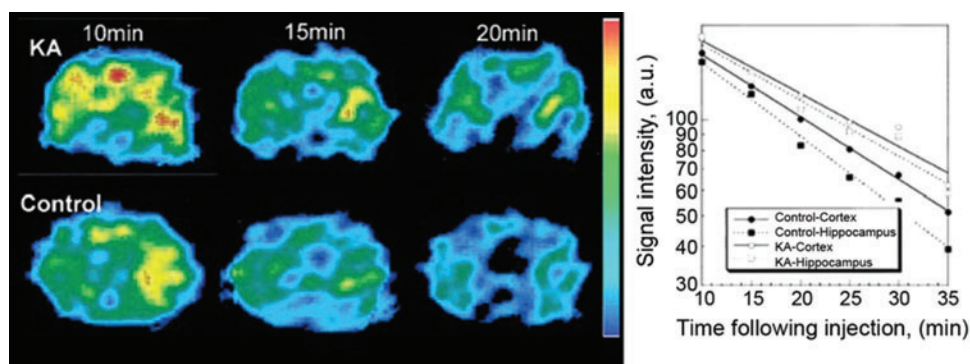**FIG. 15. EPRI of the rat brain.** *Left*: The dynamic pattern of selected transversal EPR images of the rat head 5 mm posterior to the bregma in the KA-treated and control groups at different times after injection of nitroxyl radicals (MC-PROXYL). *Right*: Pharmacokinetic curves for brain regions. The cortical half-lives of MC-PROXYL in the control and KA groups were 18.0 ± 1.2 and 19.2 ± 0.7 min, respectively, whereas the hippocampal half-lives of MC-PROXYL in the control and KA groups were 10.4 ± 0.8 and 15.9 ± 0.7 min, respectively. [Adapted from Yokoyama *et al.* (190).] KA, kainic acid. Color images are available online.

seizures induced by kainic acid, the half-life of the EPR signal of the nitroxyl radical MC-PROXYL was longer in the hippocampus than in the cortex, indicating a lower reducing ability of the hippocampus.

These observations were confirmed by the injection of diamagnetic acyl-protected hydroxylamine ACP, which undergoes intracellular oxidation to a nitroxyl radical (188). In this case, the authors detected EPR signal and an increase in its intensity in the hippocampus and striatum of kainic acid-treated animals, but not in the cortex. In other studies, the same authors treated animals with neuroleptics known to induce oxidative stress in the brain and analyzed the tissue redox status using MC-PROXYL (187, 189, 191). The brain tissues exhibited lower reducing capacity of the injected nitroxyl probe. This decrease in reducing capacity was also observed in elderly rats compared with young individuals kept under standard conditions (61, 140, 191).

One of the most widely used models for the induction of oxidative stress in the brain is experimental ischemic–reperfusion injury caused by reversible occlusion of the carotid artery ("middle cerebral artery occlusion model"). This condition is accompanied by the generation of high amounts of ROS and induction of oxidative stress in the affected areas (148). Lower reducing capacity was also reported in this model using MC-PROXYL as a redox-sensitive contrast probe and nitroxyl-enhanced EPRI and MRI (77). Similar results were reported by Yokoyama *et al.* (187) in an EPRI study of a rat model of neonatal ischemia-induced reperfusion encephalopathy, using 3-(hydroxymethyl)-1-oxy-2,2,5,5-tetramethylpyrrolidine (HM-PROXYL). Treating animals with an antioxidant abolishes (removes) this effect.

Another approach to alter the tissue redox status is the induction of septic shock by i.v. injection of lipopolysaccharides (LPS) in animals. In this case, EPRI revealed that the rate and degree of reduction of the HM-PROXYL spin probe increased in all parts of the brain of LPS-treated mice (47). Pretreatment of mice with allopurinol (xanthine oxidase inhibitor) or aminoguanidine (NOS inhibitor) suppressed the effects of septic shock on the degree of HM-PROXYL reduction, which is indirect evidence of the role of $O_2^{\bullet-}$ and nitric oxide in the dynamics of nitroxyl contrast.

In 2013, a methodology for direct visualization of $O_2^{\bullet-}$ production *in vivo* in the dopaminergic area of the brain in Parkinson's disease was developed, based on the redox cycle of mito-TEMPO (2,2,6,6-tetramethyl-4[[2-(triphenylphosphonio)acetyl]amino]-1-piperidinyloxy) and its MRI contrast (195). The experiments were conducted on healthy and 1-methyl-4-phenyl-1,2,3,6-tetrahydropyridine (MPTP)-treated mice (Fig. 16). In healthy mice, the nitroxyl-enhanced MRI signal in the "substantia nigra pars compacta" (*SNpc*) was weak and short lived. The histograms suggested high reducing activity of normal brain tissues against mito-TEMPO. In MPTP-treated mice, the nitroxyl-enhanced MRI signal in the *SNpc* was strong and long lived. The histograms suggested high oxidative activity of dopaminergic tissues in the MPTP-treated brain. This nitroxyl-based MRI study demonstrated that $O_2^{\bullet-}$ is a major inducer and/or mediator of neurodegenerative damage in Parkinson's disease in mammals.

Imaging redox imbalance and oxidative stress in cancer

It is generally accepted that the redox signaling of cancer cells and tissues is different from that of normal tissues due to the hypoxic environment, increased levels of ROS (especially $O_2^{\bullet-}$), and increased amount of reducing equivalents (mainly glutathione) in tumors (16, 83, 93, 97, 143, 174, 175). The effectiveness of radiation therapy and many chemotherapeutic approaches depends on the degree of oxygenation in tumors (19, 51). A number of studies on cancer models have been published (22, 79–81, 101, 102, 119, 168).

Imaging is the preferred technique for functional diagnostics of cancer due to the heterogeneity of tumor tissues in two aspects—their redox status and oxygenation (4, 22, 175). Therefore, spatially separated images for both are preferred: (i) the distribution of nitroxyl contrast agent in the tumor and its elimination from tumor tissue; and (ii) tumor oxygenation. To achieve this goal, different approaches are used by combining EPR and MRI, and the selection of appropriate contrast probes (50, 54, 79–81, 101, 102, 127, 147, 168, 183).
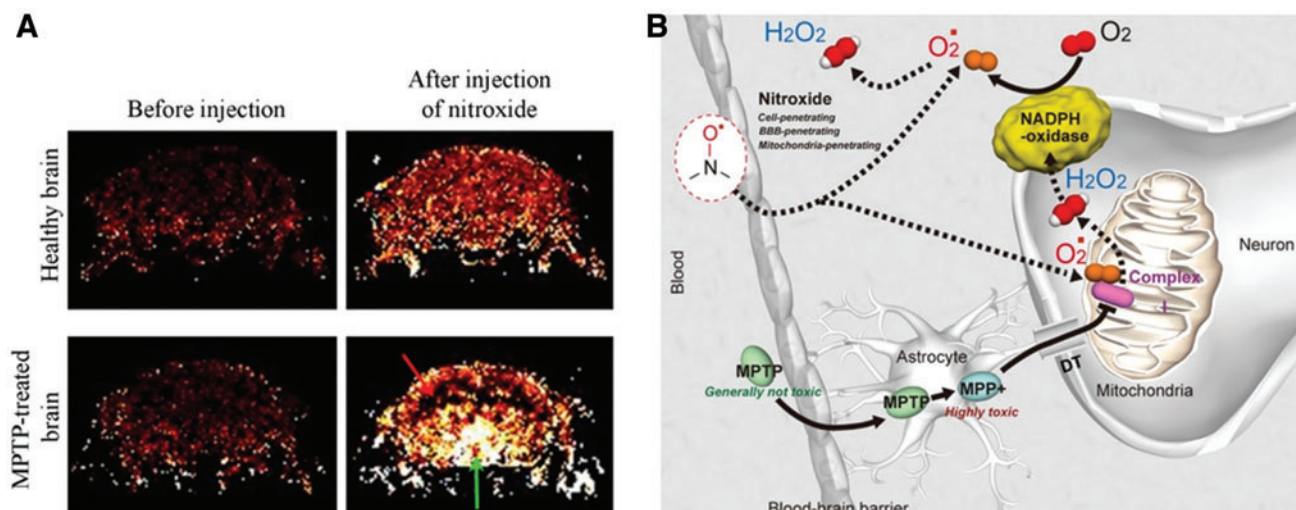
FIG. 16. Visualization of superoxide production *in vivo* in the dopaminergic area of the brain in Parkinson's disease. **(A)** Nitroxyl-enhanced MR imaging of tissue redox status in dopaminergic neurons [according to Zhelev *et al.* (195)]. Extracted nitroxyl-enhanced MRI signal in the brain of healthy and MPTP-treated mice obtained 5 min after the injection of nitroxyl contrast agent (mito-TEMPO; T_1-weighted MRI, gradient-echo). The *green arrow* indicates the *SNpc*. The *red arrow* indicates the cortex. **(B)** Molecular hypothesis for enhancement of MRI signal in MPTP-affected and oxidatively active dopaminergic neurons [according to Vila and Przedborski (182) and Zhelev *et al.* (195)]. DT, dopamine transporter; mito-TEMPO, 2,2,6,6-tetramethyl-4[[2-(triphenylphosphonio)acetyl]amino]-1-piperidinyloxy; MPP$^+$, 1-methyl-4-phenylpyridinium; MPTP, 1-methyl-4-phenyl-1,2,3,6-tetrahydropyridine. Color images are available online.

An early example of visualization and analysis of redox status of tumors in mice by nitroxyl-enhanced MRI and EPRI using carbamoyl-PROXYL as a redox-sensitive contrast agent is presented in Figure 8 (119). The authors of this study suggested that the rate of reduction of the nitroxyl radical carbamoyl-PROXYL in tumor tissue is higher than that in nontumor tissues based on the increased levels of endogenous reducing equivalents in tumor cells (mainly glutathione and glutathione-dependent antioxidants), in addition to the presence of hypoxia in tumors. Similar opinions have been expressed by other authors using carboxy-PROXYL or carbamoyl-PROXYL as contrast probes (79–81, 101, 102, 127, 183).

In vivo studies in tumor-bearing animals using ^{13}C-dehydroascorbate as an endogenous redox sensor and hyperpolarized MRI revealed that tumor tissues are characterized by higher levels of glutathione and ascorbate than normal tissues of healthy animals (90, 91). However, the authors noted that the ratio of oxidized/reduced forms of the two substances is in favor of the oxidized form in the tumor tissue and in favor of the reduced form in the normal tissues. This suggested that the reducing capacity of normal (healthy) tissues is higher than that of tumor tissues.

Roshchupkina *et al.* (150) reported a unique approach to determine the amount of reduced glutathione in isolated cancer cells and tissues by EPR spectroscopy, using two ^{15}N-labeled nitroxyl rings connected by a disulfide bridge. The EPR spectrum of the biradical differs from that of the monomer nitroxyl radical, which enables monitoring of the reaction of the probe with reduced glutathione.

In our recent studies, we used several nitroxyl radicals as redox sensors to visualize and analyze the tissue redox status in cancer tissues *in vivo* using MRI on animals: (i) SLENU—highly hydrophobic, cell-penetrating, and DNA-alkylating; (ii) TEMPOL—amphiphilic, cell-penetrating; and (iii) carbamoyl-PROXYL—hydrophilic and very low/non-penetrating in living cells and tissues (6, 194, 197, 198). A strong and long-lived nitroxyl-enhanced MRI signal was detected in the cancer tissues, and a relatively strong and long-lived signal was detected in the surrounding tissues of cancer-bearing mice (Fig. 17). In contrast, a short-lived nitroxyl-enhanced MRI signal was detected in the tissues of healthy mice. This suggested that cancer and noncancer tissues of cancer-bearing animals are characterized by high oxidative activity toward nitroxyl radicals, whereas tissues of healthy animals are characterized by high reducing activity. It should be noted that SLENU was the most appropriate nitroxyl probe to evaluate tissue redox status *in vivo* due to its easy intracellular delivery and prolonged retention in the tissues. In addition, our recent EPR study on cultured cells with different proliferative indexes demonstrated that EPR signal decay is well correlated with proliferating activity (199). The slowest rate of EPR signal attenuation was detected in rapidly proliferating cancer cells, with a higher rate in slowly proliferating noncancer cells and the highest rate in nonproliferating cells.

Imaging redox imbalance and oxidative stress in the kidneys

Hirayama *et al.* (73) used mice with acute renal failure due to ischemia–reperfusion and noted a slower decrease in EPR signal of carbamoyl-PROXYL than that in controls. This result can be explained by the induction of oxidative stress in the kidneys of mice with impaired renal function. The same group also published an EPRI study of the redox status of renal tissues in mice with hypertension induced by ligation of the right renal artery (74). In mice with hypertension, the half-life of the nitroxyl-enhanced EPR signal was longer than that in healthy mice. Treatment of mice with azelnidipine (a
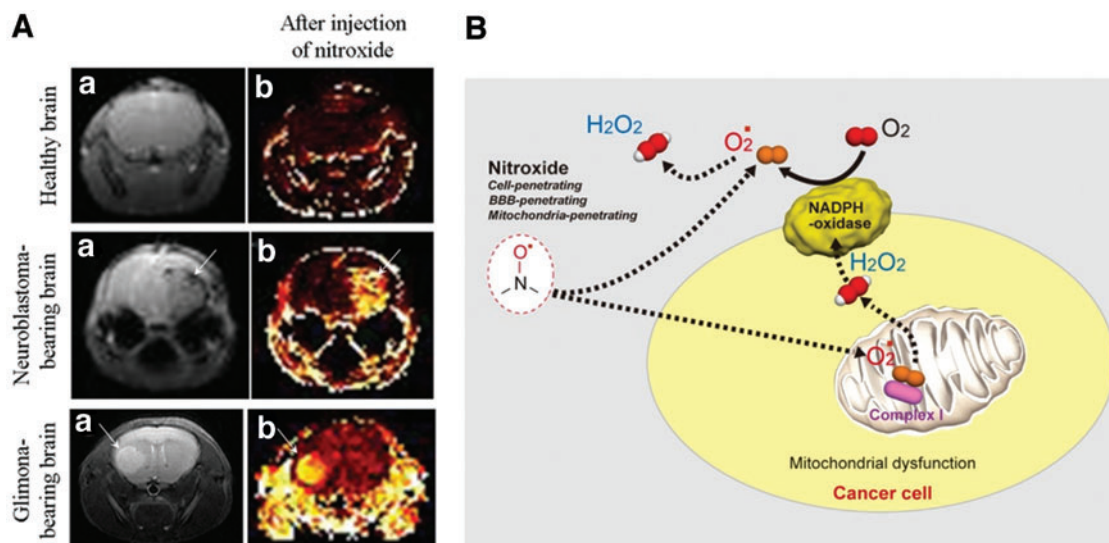
FIG. 17. Nitroxyl radicals as redox sensors to visualize and analyze the tissue redox status in cancer tissues. (A) Typical MR images of healthy brain and cancer-bearing brain of mice: **(A.a)** MR images of the mouse brain; **(A.b)** extracted nitroxyl-enhanced MRI signal obtained 6 min after the injection of nitroxyl radicals (SLENU). The *arrows* indicate the tumor area. **(B)** Molecular hypothesis for increased MRI signal in metabolically (oxidatively) active cancer cells and tissues. SLENU, TEMPO-labeled nitrosourea [according to Zhelev *et al.* (194) and Bakalova *et al.* (6)]. Color images are available online.

calcium channel blocker) for 2 weeks improved the reducing ability of the kidneys and shortened the life of the nitroxyl radicals. The same group also used another model of renal dysfunction, Nrf2-deficient mice with lupus-like autoimmune nephritis (75). The fourfold longer half-life of EPR signal of carbamoyl-PROXYL in the injured tissues of Nrf2-deficient elder mice compared with that of young wild-type mice was due to the combination of transcription factor deficiency and aging. The authors suggested that a lower reducing ability plays a role in the development of autoimmune nephritis.

Carbamoyl-PROXYL and EPRI were also applied to redox imaging of the kidneys of a murine model of streptozotocin-induced diabetes (120, 158, 161, 162, 176). These studies reported faster reduction of the nitroxyl probe in the kidneys of diabetic mice. It is generally accepted that diabetes is accompanied by the development of oxidative stress in tissues, with ROS playing a significant role in the pathogenesis of the disease (88, 149). However, it is unclear why oxidative stress in the kidneys leads to a delay in some cases (73–75, 161) and to acceleration of the EPR signal attenuation of the nitroxyl probe in others (120, 158, 161, 162, 176).

Brasch *et al.* (14) investigated the dynamics of nitroxyl-enhanced MRI in the healthy animals and animals with experimental renal ischemia and hydronephritis, using an amphiphilic nitroxyl radical 4-[(3-carboxy-1-oxopropyl) amino]-2,2,6,6-tetramethyl-1-piperidinyloxy (TES). Increased contrast was found in damaged kidneys compared with kidneys in healthy animals. Renal ischemia and hydronephritis are accompanied by the induction of high oxidative stress in the kidneys due to mitochondrial dysfunction, and production of inflammatory factors and ROS/reactive nitrogen species (7, 92, 110, 151, 152, 165). Decreased perfusion in damaged kidneys has also been reported in many studies (7, 116), which implies that penetration of this organ by contrast agent is difficult. Therefore, the increased contrast of TES in the damaged kidney after ischemia/reperfusion is most likely a result of oxidative stress and existence of nitroxyl contrast agent mainly in a radical form.

Although a possibility of delayed or accelerated filtration of nitroxyl contrast agent in the kidneys would be the main factors that can affect the dynamics of the nitroxyl probes in this organ regardless of the redox state of the tissues, discussion about renal clearance of the past experimental model had been lacking. In models of renal dysfunction, at least one conventional contrast agent and technique, such as gadolinium-enhanced MRI, must be used to determine whether the signal dynamics in the damaged kidney are the result of an increased or decreased filtration rate.

One of the well-described models of renal dysfunction based on chronic inflammation is hypercholesterolemia-induced microvascularization in the renal cortex, and subsequent calcification that causes glomerulosclerosis and degeneration of the proximal tubules (92, 116, 152). In this experimental model, we did not detect nitroxyl-enhanced MRI signal in the kidneys of mice with hypercholesterolemia using carbamoyl-PROXYL as a contrast probe (Fig. 18) (173). However, a large decrease in renal perfusion was found using gadolinium-enhanced MRI. This suggests that the lack of nitroxyl-enhanced MRI signal of carbamoyl-PROXYL in the dysfunctional kidneys was not a result of rapid reduction of this nitroxyl radical to its diamagnetic form. In healthy mice, cell penetration of carbamoyl-PROXYL is limited *in vivo* due to the competition of this process with its relatively rapid excretion (79, 171). In contrast, using a hydrophobic and cell-penetrating nitroxyl radical, mito-TEMPO, we observed a long-lived nitroxyl-enhanced MRI signal in the kidneys of mice with hypercholesterolemia and short-lived MRI signal in the kidneys of healthy mice (Fig. 19) (103).

In this case, the probe was retained in the renal tissues, and the higher intensity of MRI signal of mito-TEMPO in the kidneys of mice with hypercholesterolemia was mainly due to the lower reducing capacity of inflamed renal tissues than
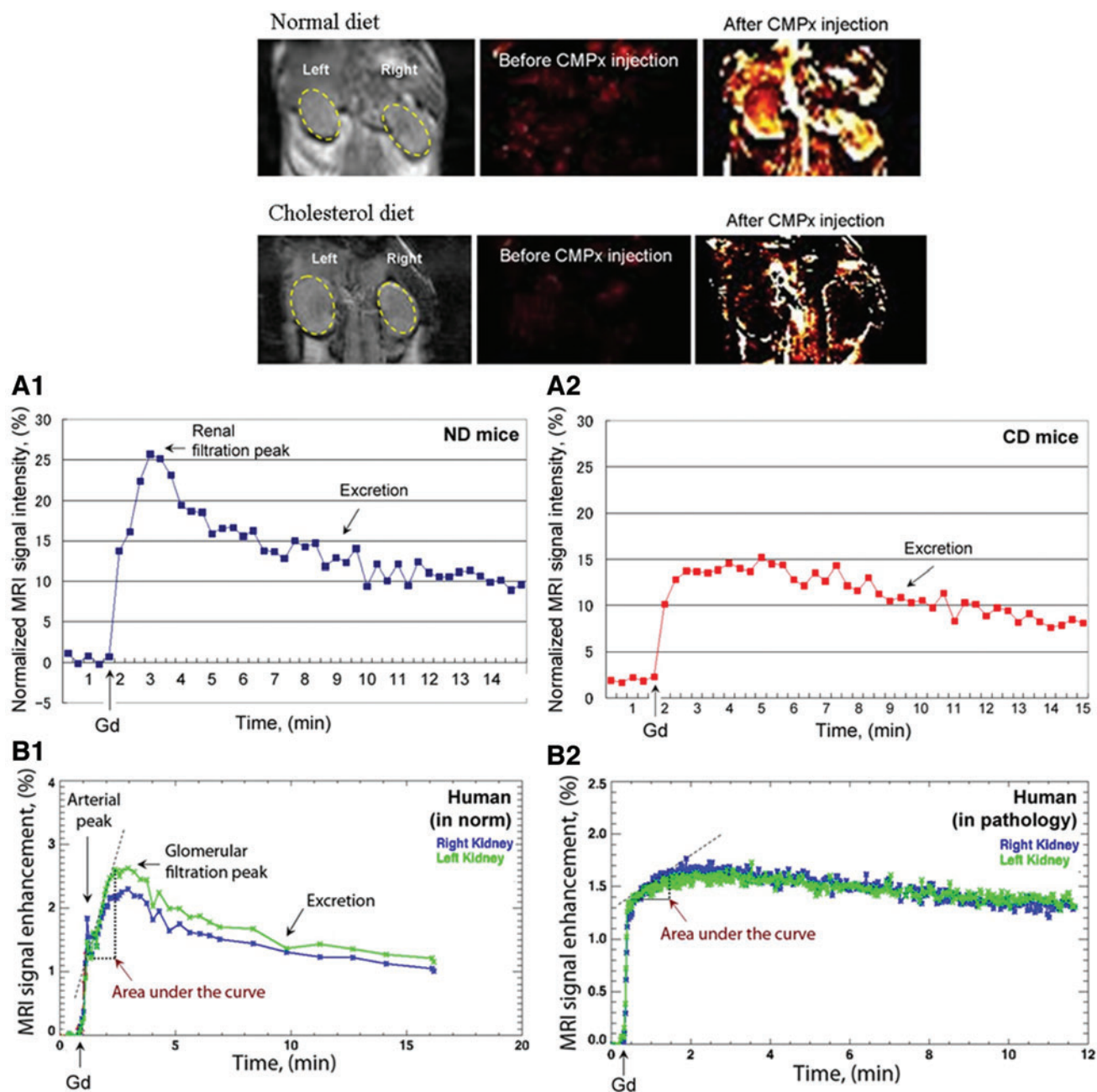
FIG. 18. Nitroxyl-enhanced MRI of the kidney in mice on a ND or high CD using carbamoyl-PROXYL as a contrast probe: black and white images: T_1-weighted MR images of the kidney before the injection of carbamoyl-PROXYL. Color images: extracted MRI signal intensity normalized to the averaged baseline level (before the injection of carbamoyl-PROXYL). (A) Kinetic curves of normalized MRI signal intensity in kidneys before and after the injection of Gd-DTPA in ND mice (A1) or CD mice (A2). The data are the mean from four animals (standard error did not exceed 20%). ImageJ software was used for data processing. (B) Typical kinetic curves of Gd-enhanced MRI in the ROI within the kidney of healthy humans (B1) and humans with renal pathology (B2). CHOP-fMRU software was used for data processing of the postcontrast T_1 VIBE Dynamic sequence in the coronal plane during excretory MR urography. CD, cholesterol diet; ND, normal diet [according to Tomizawa et al. (173)]. Color images are available online.

the kidneys of healthy mice. This approach enables also the assessment of the effectiveness of antilipidemic drugs (Fig. 19).

The studies described above demonstrate the potential of nitroxyl probes for translational studies on functional MR urography (35, 38, 145). The major problem of this

clinical approach is the use of contrast substances that increase the risk of intoxication in patients with impaired renal filtration. The efforts of clinicians are focused in two directions: (i) development of noncontrast methods for visualization and assessment of renal dysfunction; and (ii) development of nontoxic or low-toxicity contrast
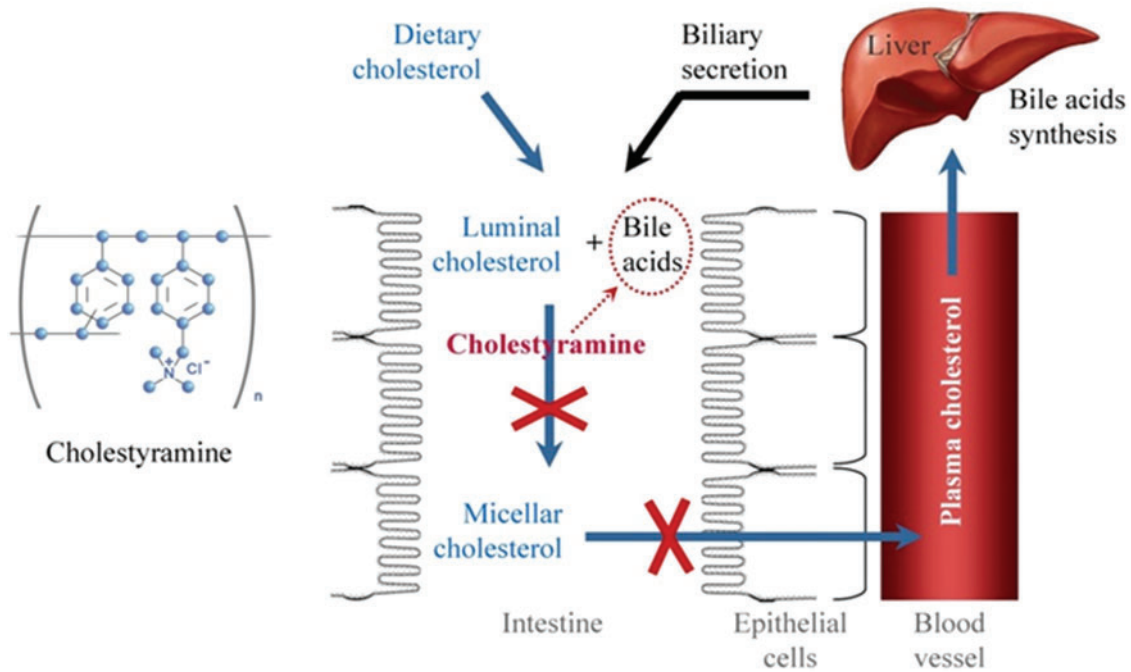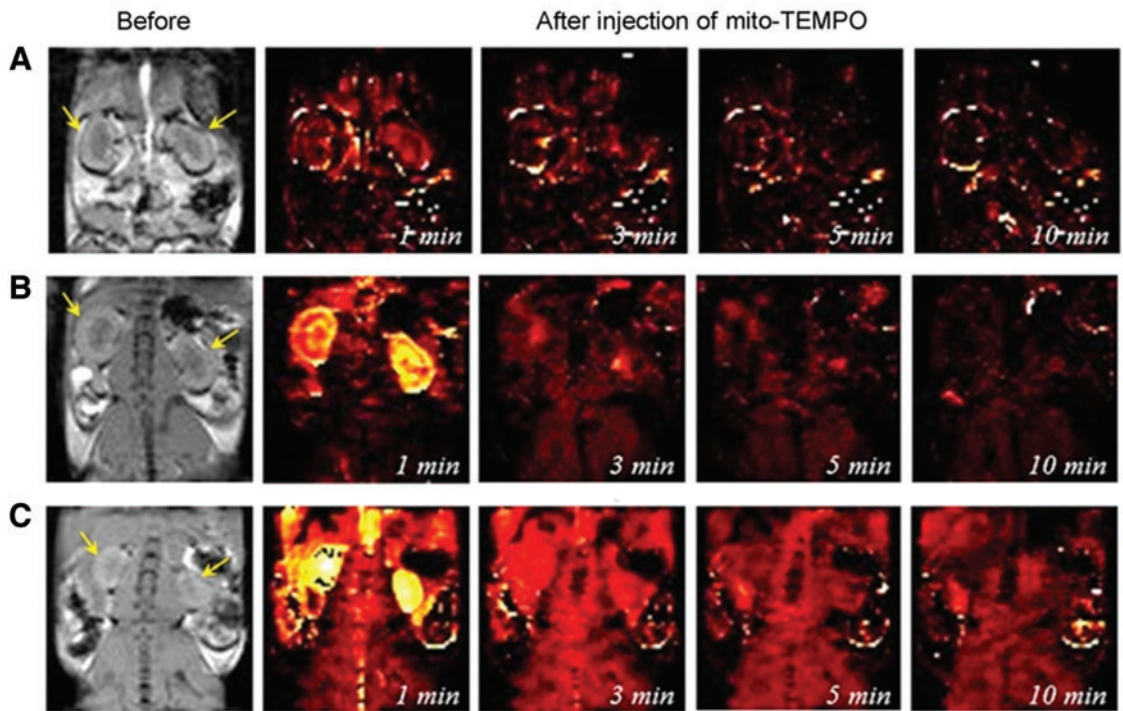
FIG. 19. Nitroxyl-enhanced MRI of the kidney in mice on a ND or high CD using mito-TEMPO as a contrast probe: black and white images: T_1-weighted MR images of the kidney before the injection of mito-TEMPO. Color images: extracted MRI signal intensity normalized to the averaged baseline level (before the injection of mito-TEMPO): **(A)** ND; **(B)** cholesterol plus cholestyramine diet; **(C)** CD. The *yellow arrows* indicate the kidneys. Structural formula and mechanism of reduced plasma cholesterol by the bile acid sequestrant cholestyramine [according to Lazarova *et al.* (103)]. Color images are available online.

substances for functional urography (5, 8, 128). Low-toxicity nitroxyl-based contrast probes have the potential to meet the second condition. The structures of several TEMPO analog nitroxyl probes commonly used are shown in Supplementary Figure S2.

Trials of redox imaging in the skin and other organs

The skin is the perfect target for EPRI of oxidative stress due to necessity of low depth of microwave penetration, which enables the use of S-band (2–3 GHz) for *in vivo*

imaging or even X-band for isolated samples. After topical application of nitroxyl, its distribution in the skin and the redox status of the different layers can be visualized using a simple EPR spectral-spatial two-dimensional image. The potential of this approach has been well demonstrated in studies of human skin *in vivo* (95, 109, 154, 181), revealing opportunities for the investigation and diagnosis of skin pathologies, aging, and photo-induced damage.

Fuchs *et al.* (45) investigated the diffusion of several nitroxyl radical compounds into the skin of mice, and reported that lipophilic nitroxyl-labeled estradiol penetrates the dermis faster than hydrophilic nitroxyl-labeled procaine. The same group used X-band EPR to analyze the stability of nitroxyl compounds in skin biopsies, homogenates, and keratinocytes, and in the induction of erythema (43, 44). The rate of attenuation of the EPR signal of nitroxyl compounds increases in the following order: imidazoline < pyrrolidine < piperidine < oxazolidine (43). Thus, the nitroxyl compounds used either do not cause erythema, or the irritation is defined as moderate even at high concentrations (100 mM) (44). In this regard, one of the most popular nitroxyl radicals, TEMPOL, is used in ongoing clinical trials as a radioprotector for topical application, which prevents hair loss during radiation therapy of patients with malignancies (126).

Ultraviolet-induced overproduction of ROS in the skin has been also demonstrated using spin traps (85, 86) or nitroxyl probes (69–72, 167, 168, 170).

Another model of oxidative stress *in vivo* is the intoxication of animals with iron *via* the induction of Fenton reactions. Phumala *et al.* (144) conducted an EPR study on iron-loaded mice, and found that the EPR signal of carbamoyl-PROXYL in the liver decreased significantly faster than that in healthy animals, but this was suppressed by the pretreatment of mice with desferrioxamine or trolox. Similar dynamics of the EPR signal of carbamoyl-PROXYL were observed in the liver of animals exposed to ionizing radiation (131).

Han *et al.* (68) and Ahsan *et al.* (1) found that attenuation of the EPR signal of the nitroxyl radical CAT1 (4-trimethylammonium-2,2,6,6-tetramethylpiperidine-*N*-oxyl or choline-TEMPO) was significantly accelerated in the lungs of mice after intratracheal administration of burned diesel fuel particles. The effects of diesel particles were suppressed by scavengers of hydroxyl radicals and thiol-containing proteins (1, 68). It should be noted that CAT1 does not penetrate through cell membranes and cannot be an indicator of the intracellular redox status of alveolocytes. The dynamics of the EPR signal of CAT1 are most likely affected by extracellular substances such as ROS generated by the ''oxidative burst'' of macrophages in the pulmonary loci with concentrated diesel particles.

Leonard *et al.* (104) observed a significant delay in the reduction of the nitroxyl probe TEMPOL in the lungs of asbestos-treated mice. Caia *et al.* (15) reported that mice exposed to cigarette smoke had lower reducing capacity toward the carbamoyl-PROXYL in almost all abdominal organs.

Togashi *et al.* (172) also used the carbamoyl-PROXYL and EPRI system to analyze the redox status of the liver in carbon tetrachloride (CCl$_4$)-treated mice. They reported that the rate of nitroxyl reduction was significantly slower in CCl$_4$-treated mice than in untreated controls. Another EPR study of mice with hepatic injury (as a result of ischemia–

reperfusion) reported that blockade of Ca^{2+}/calmodulin by the calmodulin antagonist CV159 resulted in faster attenuation of the EPR signal of carbamoyl-PROXYL in treated animals than in untreated controls (96).

Possibilities of redox imaging of biological objects using spin trapping

EPR spin-trapping techniques are attractive modalities, as they enable the detection of specific ROS. The *in vivo* detection of free radicals by spin trapping was previously demonstrated in mice irradiated with ionizing radiation, which induces the overproduction of ROS and severe oxidative stress (66, 67). Visualization of O$_2^{\bullet-}$ and hydroxyl radicals can be improved by developing more stable spin traps and the use of ^{15}N-substituted spin trapping, which may increase the sensitivity and resolution by reducing the number of lines in the EPR spectrum (94). However, imaging biological ROS using a combination of *in vivo* spin trapping and EPRI and/or MRI is difficult at this time.

Over the last decade, an immunospin capture method was developed based on the concept that DMPO (5,5-dimethyl-1-pyrroline-*N*-oxide) reacts with protein radicals, and the products can be identified immunologically with high specificity. Mason (115) developed antibodies against DMPO–protein radical adducts (anti-DMPO) that can be used in immunoblotting, immunohistochemistry, immunofluorescence, and flow cytometric analyses. This approach significantly extends the benefits of using spin traps in the detection of redox-active substances because immunological techniques are characterized by high sensitivity (17, 115, 146). Immunospin traps have been used to detect DMPO–protein products of myoglobin and hemoglobin, as well as ROS adducts in isolated mitochondria, cells, and tissue samples (17, 26, 59, 60, 100).

However, the method is only applicable *in vitro* and has limitations: (i) it cannot detect free radicals, such as O$_2^{\bullet-}$ and hydroxyl radical, and only enables the identification of modified protein adducts; (ii) multiple antibodies specific for different types of protein adducts are required to cover the full range of targets to ensure high sensitivity of the analysis.

Redox imaging of biological objects using cyclic hydroxylamines

At the end of the last century, diamagnetic forms of nitroxyl radicals, cyclic hydroxylamines (Fig. 20), were found to be suitable for the detection of O$_2^{\bullet-}$ in biological objects *in vitro* and *in vivo* (27, 29–33). Hydroxylamines are diamagnetic and have no EPR/MRI contrast. They are oxidized by ROS (in particular, by O$_2^{\bullet-}$) with the formation of stable paramagnetic substances, nitroxyl radicals, with a half-life of up to several hours in isolated model and biological systems (27, 29–31). This enables them to be registered by EPR spectroscopy, EPRI, and MRI in the case of oxidation.

Compared with nitrons, cyclic hydroxylamines react much faster with O$_2^{\bullet-}$ radicals, with a reaction rate constant of $\sim 10^3$–10^4 $M^{-1} \cdot s^{-1}$ at pH = 7.4. This favors the competition of hydroxylamines with cellular antioxidants and improves the efficiency of detection of intracellular O$_2^{\bullet-}$ (30). For this reason, hydroxylamines can be used at relatively low concentrations (0.05–1 mM), which minimizes their side effects in biological systems. Another advantage of cyclic
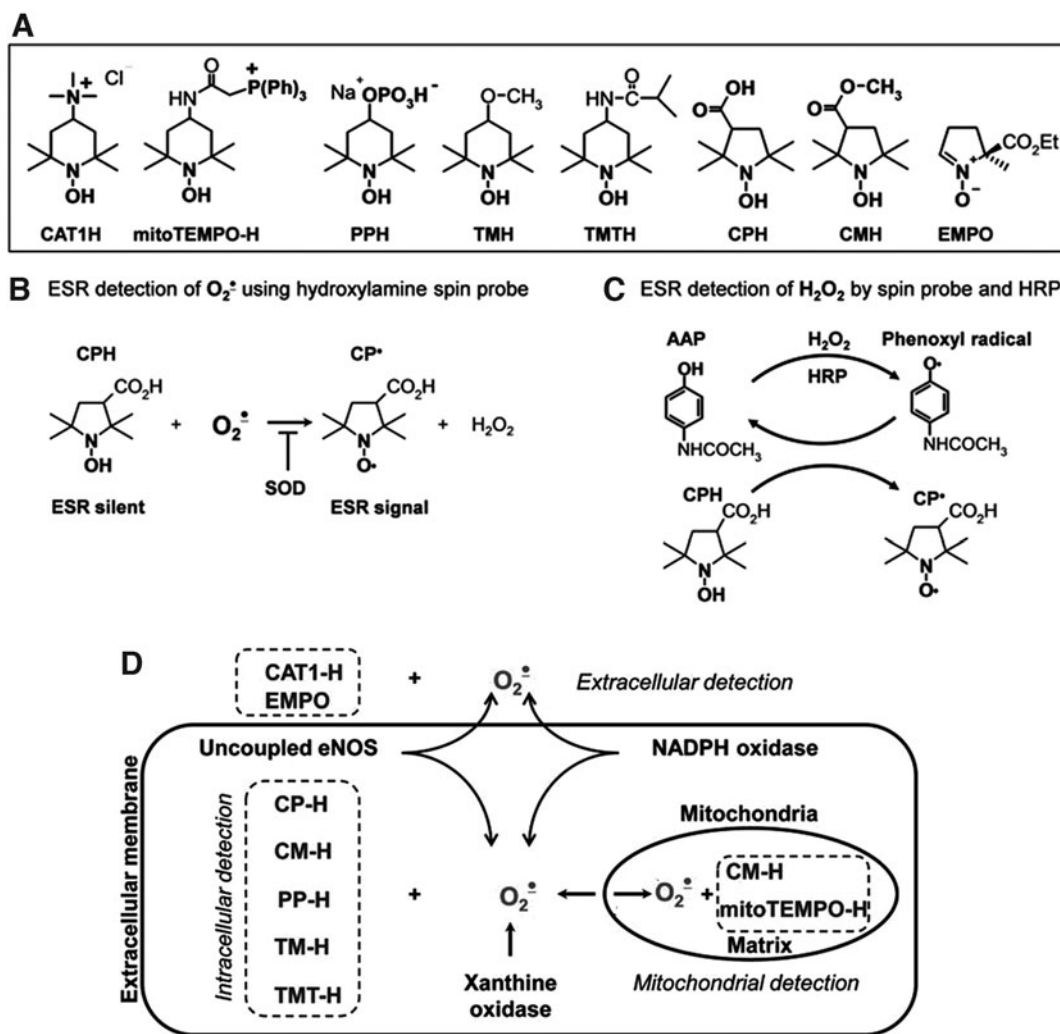
FIG. 20.   **Detection of mitochondrial and cellular ROS by hydroxylamine probes.** (**A**) Chemical structures of hydroxylamine probes. (**B**) EPR detection of cellular superoxide using hydroxylamines. (**C**) EPR detection of hydrogen peroxide using hydroxylamines and HRP. (**D**) General scheme of EPR detection of superoxide in extracellular, intracellular, or mitochondrial compartments using cyclic hydroxylamine spin probes. HRP, horseradish peroxidase; Rot, rotenone. [Adapted from Dikalov *et al.* (32) and Dikalov and Harrison (31).]

hydroxylamines is that they react with $O_2^{•-}$ in a single chemical reaction. This reduces the potential artifacts arising from multistage redox reactions typical of other redox-sensitive probes (fluorescent and chemiluminescent) (42). For example, unlike lucigenin, cyclic hydroxylamines do not have the so-called ''redox cycling,'' and no additional ROS were generated (114).

Dikalov *et al.* (32) investigated the dynamics of the EPR signal of cyclic hydroxylamines in biological systems. This study supports the essential role of the hydrophobic (amphiphilic) nature of cyclic nitroxyl probes, and their penetration into cells in the dynamics of their contrast properties and their ability to be used as intracellular or extracellular redox sensors. The authors demonstrated that cationic and membrane-impermeable CAT1-H (hydroxylamine form of CAT1) detects only extracellular $O_2^{•-}$ released from live cells or extramitochondrial $O_2^{•-}$ released from isolated mitochondria. In contrast, cell-penetrating MCP-H (hydroxylamine form of MC-PROXYL), PP-H (hydroxylamine form of 4-phosphonooxy-TEMPO), and mito-TEMPO-H (hy-

droxylamine form of mito-TEMPO) are suitable for the detection of intracellular and extracellular ROS. PP-H is thought to accumulate in cells by active transport, MCP-H accumulates predominantly in the cytoplasm, and mito-TEMPO-H is mitochondrially targeted and localized predominantly in mitochondria (32, 84). MCP-H may also accumulate in mitochondria.

MCP-H gives a strong EPR signal in cells treated with phorbol-12-myristate-13-acetate, stimulating the production of cytoplasmic $O_2^{•-}$, whereas the signal of mito-TEMPO-H is weaker in this case (25, 32). In contrast, rotenone-induced generation of mitochondrial $O_2^{•-}$ results in a strong EPR signal induced by mito-TEMPO-H and MCP-H, but not PP-H (32). Thus, relatively accurate information on the origin of ROS (extracellular, intracellular, or mitochondrial) can be obtained using appropriate selection of cyclic hydroxylamine.

In general, the advantage of cyclic hydroxylamines is in their use for direct detection of ROS in cells, subcellular fractions, and tissue homogenates at room temperature by examining the accumulation of the nitroxyl radical by EPR

spectroscopy. Low-temperature EPR is suitable for detecting ROS in intact tissues. For this purpose, the samples were incubated in physiological saline containing cyclic hydroxylamines and then frozen in liquid nitrogen, stored at –80°C, and later analyzed at a low temperature (9, 28).

Kozlov *et al.* (98) injected cyclic hydroxylamines into young and old rats, and monitored the appearance and increase in EPR signal in tissue homogenates isolated from various organs *ex vivo*. The authors found that the oxidative capacity of the blood, skeletal muscle, lungs, and heart increases significantly with age, but does not change the redox status of the intestine, brain, liver, or kidneys. Cyclic hydroxylamines have been used in model systems and isolated biological objects, including blood and biopsy samples from patients with numerous diseases (9, 113). However, no use of these spin probes in nitroxyl-enhanced EPRI or MRI has been reported in intact animals *in vivo*.

Other contrast substances and techniques for redox imaging and perspectives on cyclic nitroxyl radicals

There are many contrast media that can give detectable products reflecting the localization and level of a particular target investigated; that is, the redox-active molecular species or the biological redox environments. The most of *in vitro* detection of these contrasts (*e.g.*, fluorescence) is feasible with high sensitivity and resolution, but *in vivo* detection is highly difficult to implement. Another group of contrast agents (*e.g.*, nuclear and ultrasound) can achieve *in vivo* detection with high sensitivity, although the resolution is low. In general, nuclear-labeled contrast agents can provide indirect information about the tissue redox status, which can be given as a result of biochemical and physiological processes such as glycometabolism, O_2 consumption, hypoxia, and cell retention depending on the cytoplasmic redox potential. In addition, such radioactive contrast agents may increase the risks for the patient. Of note, the above-mentioned methodologies enable assessment of the redox status of the biological object based on the information obtained for one or several redox-active compounds. Thus, the discussions and conclusions in studies are often contradictory.

At present, efforts are focused on mapping the redox status of tissues and organs in intact organisms. The perfect methodology should provide direct and noninvasive detection of the redox status of the target organ *in vivo*. In this context, the perfect redox-sensitive contrast substances should meet the following conditions:

- Ability to penetrate the cells and BBB, if possible;
- ability to provide information about the equilibrium between the intracellular oxidizers and reducers for the total redox status of cells and tissues, not only for the status of a certain redox-active compound (*e.g.*, its oxidized or reduced form);
- be nontoxic or low-toxic *in vivo*;
- be rapidly excreted through the living organism;
- have high contrast and enable imaging with high resolution.

Cyclic nitroxyl radicals have a relatively low toxicity (safer than gadolinium and manganese complexes) and are not mutagenic (2, 21). They are characterized by favorable biomedical effects such as anticancer effects, regulation of body weight, protection against ischemia–reperfusion injury, protective effects against cataract, sensitizing cancer cells and tissues to ionizing radiation, and protecting normal cells and tissues (34, 107, 163, 164, 200). Moreover, some cyclic nitroxyl radicals are undergoing clinical trials for topical applications (192). This confirms the potential of nitroxyl radicals as new contrast substances for redox imaging in translational studies on humans using MRI. However, this can only be achieved after many preliminary studies on experimental animals to select the most appropriate nitroxyl probes for redox imaging, route of administration, and safe doses. This will provide a new opportunity for MRI/EPRI analysis of metabolic pathways, accompanied by minor changes in the redox status of biological objects and induction of oxidative stress.

Conclusion

Redox imaging is a useful tool to detect an abnormal tissue redox status such as disordered oxidative stress or tumor hypoxia. Data from nitroxyl-enhanced MRI/EPRI *in vivo* must be considered and interpreted carefully because the kinetics of the signal in the target tissue or organ depend on a number of factors: (i) life time of nitroxyl radicals in the bloodstream; (ii) penetration through cell membranes and localization in target cells and tissues; (iii) rate of excretion from the organism; (iv) selection of appropriate ROI; and (v) use of healthy individuals as controls. A suitable chemical and/or biological nitroxyl radical contrast agent will provide useful information for translational theranostic applications in the target organ/tissue.

Acknowledgments

Authors' Contributions

K-i.M., I.N., Z.Z., and R.B. contributed to writing original draft of the article; K-i.M., I.N., Z.Z., and R.B. contributed to writing review and editing; I.A. supervised; I.A. and R.B. performed funding acquisition. All authors have read and agreed to the published version of the article.

Author Disclosure Statement

No competing financial interests exist.

Funding Information

Supplementary Material

Supplementary Figure S1
Supplementary Figure S2

References

1. Ahsan MK, Nakamura H, Tanito M, Yamada K, Utsumi H, and Yodoi J. Thioredoxin-1 suppresses lung injury and apoptosis induced by diesel exhaust particles (DEP) by scavenging reactive oxygen species and by inhibiting DEP-induced downregulation of Akt. *Free Radic Biol Med* 39: 1549–1559, 2005.
2. Ankel EG, Lai CS, Hopwood LE, and Zivkovic Z. Cytotoxicity of commonly used nitroxide radical spin probes. *Life Sci* 40: 495–498, 1987.
3. Bacic G, Nilges MJ, Magin RL, Walczak T, and Swartz HM. In vivo localized ESR spectroscopy reflecting metabolism. *Magn Reson Med* 10: 266–272, 1989.
4. Bacic G, Pavicevic A, and Peyrot F. In vivo evaluation of different alterations of redox status by studying pharmacokinetics of nitroxides using magnetic resonance techniques. *Redox Biol* 8: 226–242, 2016.
5. Bagshaw SM and Culleton BF. Contrast-induced nephropathy: epidemiology and prevention. *Minerva Cardioangiol* 54: 109–129, 2006.
6. Bakalova R, Zhelev Z, Aoki I, and Saga T. Tissue redox activity as a hallmark of carcinogenesis: from early to terminal stages of cancer. *Clin Cancer Res* 19: 2503–2517, 2013.
7. Baligand C, Qin H, True-Yasaki A, Gordon JW, von Morze C, Santos JD, Wilson DM, Raffai R, Cowley PM, Baker AJ, Kurhanewicz J, Lovett DH, and Wang ZJ. Hyperpolarized 13 C magnetic resonance evaluation of renal ischemia reperfusion injury in a murine model. *NMR Biomed* 30: 10, 2017.
8. Bashir MR, Jaffe TA, Brennan TV, Patel UD, and Ellis MJ. Renal transplant imaging using magnetic resonance angiography with a non-nephrotoxoc contrast agent. *Transplantation* 96: 91–96, 2013.
9. Berg K, Ericsson M, Lindgren M, and Gustafsson H. A high precision method for quantitative measurements of ROS in frozen biopsies. *PLoS One* 9: e90964, 2014.
10. Berliner LJ. The evolution of biomedical EPR (ESR). *Biomed Spectrosc Imaging* 5: 5–26, 2016.
11. Blinco JP, Hodgson JL, Morrow BJ, Walker JR, Will GD, Coote ML, and Bottle SE. Experimental and theoretical studies of the redox potentials of cyclic nitroxides. *J Org Chem* 73: 6763–6771, 2008.
12. Bobko AA, Kirilyuk IA, Grigor'ev IA, Zweier JL, and Khramtsov VV. Reversible reduction of nitroxides to hydroxylamines: the roles for ascorbate and glutathione. *Free Radic Biol Med* 42: 404–412, 2007.
13. Brasch RC. Work in progress: methods of contrast enhancement for NMR imaging and potential applications. A subject review. *Radiology* 147:781–788, 1983.
14. Brasch RC, Nitecki DE, Brant-Zawadzki M, Enzmann DR, Wesbey GE, Tozer TN, Tuck LD, Cann CE, Fike JR, and Sheldon P. Brain nuclear magnetic resonance imaging enhanced by paramagnetic nitroxide contrast agent: preliminary report. *Am J Roentgenol* 141: 1019–1023, 1983.
15. Caia GL, Efimova OV, Velayutham M, El-Mahdy MA, Abdelghany TM, Kesselring E, Petryakov S, Sun Z, Samouilov A, and Zweier JL. Organ specific mapping of in vivo redox state in control and cigarette smoke-exposed mice using EPR/NMR co-imaging. *J Magn Reson* 216: 21–27, 2012.
16. Chaiswing L, Zhong W, Liang Y, Jones DP, and Oberley TD. Regulation of prostate cancer cell invasion my modulating of extra- and intracellular redox balance. *Free Radic Biol Med* 52: 452–461, 2012.
17. Chen X, Gawryluk JW, Wagener JF, Ghribi O, and Geiger JD. Caffeine blocks disruption of blood brain barrier in a rabbit model of Alzheimer's disease. *J Neuroinflammation* 5: 12, 2008.
18. Chiche J, Brahimi-Horn MC, and Pouysségur J. Tumour hypoxia induces a metabolic shift causing acidosis: a common feature in cancer. *J Cell Mol Med* 14: 771–794, 2010.
19. Colliez F, Gallez B, and Jordan BF. Assessing tumor oxygenation for predicting outcome in radiation oncology: a review of studies correlating tumor hypoxic status and outcome in the preclinical and clinical settings. *Front Oncol* 7: 10, 2017.
20. Cotrim AP, Hyodo F, Matsumoto K, Sowers AL, Cook JA, Baum BJ, Krishna MC, and Mitchell JB. Differential radiation protection of salivary glands versus tumor by Tempol with accompanying tissue assessment of Tempol by magnetic resonance imaging. *Clin Cancer Res* 13: 4928–4933, 2007.
21. Damiani E, Greci L, and Hrelia P. Cyto- and genotoxic effects of novel aromatic nitroxide radicals in vitro. *Free Radic Biol Med* 28: 330–336, 2000.
22. Davis RM, Mitchell JB, and Krishna MC. Nitroxides as cancer imaging agents. *Anticancer Agents Med Chem* 11: 347–358, 2011.
23. Davis RM, Sowers AL, DeGraff W, Bernardo M, Thetford A, Krishna MC, and Mitchell JB. A novel nitroxide is an effective brain redox imaging contrast agent and in vivo radioprotector. *Free Radic Biol Med* 51: 780–790, 2011.
24. Deguchi H, Yasukawa K, Yamasaki T, Mito F, Kinoshita Y, Naganuma T, Sato S, Yamato M, Ichikawa K, Sakai K, Utsumi H, and Yamada K. Nitroxides prevent exacerbation of indomethacin-induced gastric damage in adjuvant arthritis rats. *Free Radic Biol Med* 51: 1799–1805, 2011.
25. Deschacht M, Horemans T, Martinet W, Bult H, Maes L, and Cos P. Comparative EPR study of different macrophage types stimulated for superoxide and nitric oxide production. *Free Radic Res* 44: 763–772, 2010.
26. Deterding LJ, Ramirez DC, Dubin JR, Mason RP, and Tomer KB. Identification of free radicals on hemoglobin from its self-peroxidation using mass spectrometry and immunospin trapping: observation of a histidinyl radical. *J Biol Chem* 279: 11600–11607, 2004.
27. Dikalov S, Fink B, Skatchkov M, and Bassenge E. Comparison of glyceryl trinitrate-induced with pentaerythrityl tetranitrate- induced in vivo formation of superoxide radicals: effect of vitamin C. *Free Radic Biol Med* 27: 170–176, 1999.
28. Dikalov S, Griendling KK, and Harrison DG. Measurement of reactive oxygen species in cardiovascular studies. *Hypertension* 49: 717–727, 2007.
29. Dikalov S, Skatchkov M, Fink B, and Bassenge E. Quantification of superoxide radicals and peroxynitrite in vascular cells using oxidation of sterically hindered hydroxylamines and electron spin resonance. *Nitric Oxide* 1: 423–431, 1997.
30. Dikalov SI, Dikalova AE, and Mason RP. Noninvasive diagnostic tool for inflammation-induced oxidative stress using electron spin resonance spectroscopy and an extracellular cyclic hydroxylamine. *Arch Biochem Biophys* 402: 218–226, 2002.
31. Dikalov SI and Harrison DG. Methods for detection of mitochondrial and cellular reactive oxygen species. *Antioxid Redox Signal* 20: 372–372, 2014.

32. Dikalov SI, Kirilyuk IA, Voinov M, and Grigor'ev IA. EPR detection of cellular and mitochondrial superoxide using cyclic hydroxylamines. *Free Radic Res* 45: 417–430, 2011.

33. Dikalova A, Clempus R, Lassegue B, Cheng G, McCoy J, Dikalov S, San Martin A, Lyle A, Weber DS, Weiss D, Taylor WR, Schmidt HH, Owens GK, Lambeth JD, and Griendling KK. NOX1 overexpression potentiates angiotensin II-induced hypertension and vascular smooth muscle hyperthrophy in transgenic mice. *Circulation* 112: 2668–2676, 2005.

34. Dikalova AE, Bikineyeva AT, Budzyn K, Nazarewicz RR, McCann L, Lewis W, Harrison DG, and Dikalov SI. Therapeutic targeting of mitochondrial superoxide in hypertension. *Circ Res* 107: 106–116, 2010.

35. Dong Y, Wang WP, Cao J, Fan P, and Lin X. Early assessment of chronic kidney dysfunction using contrast-enhanced ultrasound: a pilot study. *Br J Radiol* 87: 20140350, 2014.

36. Eales KL, Hollinshead KER, and Tennant DA. Hypoxia and metabolic adaptation of cancer cells. *Oncogenesis* 5: e190, 2016.

37. Eguchi A, Yoshitomi T, Lazic M, Johnson CD, Vong LB, Wree A, Povero D, Papouchado BG, Nagasaki Y, and Feldstein AE. Redox nanoparticles as a novel treatment approach for inflammation and fibrosis associated with nonalcoholic steatohepatitis. *Nanomedicine (Lond)* 10: 2697–2708, 2015.

38. El-Baz A, Fahmi R, Yuksel S, Farag AA, Miller W, El-Ghar MA, and Eldiasty T. A new CAD system for the evaluation of kidney disease using DCE-MRI. *Med Image Comput Comput Assist Invest* 9: 446–453, 2006.

39. Emoto MC, Sasaki K, Maeda K, Fujii HG, and Sato S. Synthesis and evaluation as a blood-brain barrier-permeable probe of 7-N-(PROXYL-3-yl-methyl)theophylline. *Chem Pharm Bull* 66: 887–891, 2018.

40. Emoto MC, Sato S, and Fujii HG. Development of nitroxide-based theranostic compounds that act both as anti-inflammatory drugs and brain redox imaging probes in MRI. *Magn Reson Chem* 54: 705–711, 2016.

41. Eto H, Tsuji G, Chiba T, Furue M, and Hyodo F. Non-invasive evaluation of atopic dermatitis based on redox status using in vivo dynamic nuclear polarization magnetic resonance imaging. *Free Radic Biol Med* 103: 209–215, 2017.

42. Fernandes DC, Wosniak J, Jr., Pescatore LA, Bertoline MA, Liberman M, Laurindo FR, and Santos CX. Analysis of DHE-derived oxidation products by HPLC in the assessment of superoxide production and NADPH oxidase activity in vascular systems. *Am J Physiol Cell Physiol* 292: C413–C422, 2007.

43. Fuchs J, Freisleben HJ, Podda M, Zimmer G, Milbradt R, and Packer L. Nitroxide radical biostability in skin. *Free Radic Biol Med* 15: 415–423, 1993.

44. Fuchs J, Groth N, and Herrling T. Cutaneous tolerance to nitroxide free radicals in human skin. *Free Radic Biol Med* 24: 643–648, 1998.

45. Fuchs J, Groth N, Herrling T, Milbradt R, Zimmer G, and Packer L. Electron paramagnetic resonance (EPR) imaging in skin: biophysical and biochemical microscopy. *J Invest Dermatol* 98: 713–719, 1992.

46. Fuchs J, Groth N, Herrling T, and Zimmer G. Electron paramagnetic resonance studies on nitroxide radical 2,2,5,5-tetramethyl-4-piperidin-1-oxyl (TEMPO) redox reactions in human skin. *Free Radic Biol Med* 22: 967–976, 1997.

47. Fujii H, Sato-Akaba H, Emoto MC, Itoh K, Ishihara Y, and Hirata H. Non-invasive mapping of the redox status in septic mouse by in vivo EPR imaging. *Magn Reson Med* 31: 130–138, 2013.

48. Fukuzumi S and Ohkubo K. Metal ion-coupled and decoupled electron transfer. *Cood Chem Rev* 254: 372–385, 2010.

49. Fukuzumi S, Ohkubo K, and Morimoto Y. Mechanism of metal ion-coupled electron transfer. *Phys Chem Chem Phys* 14: 8472–8484, 2012.

50. Gallez B, Bacic G, Goda F, Jiang J, O'Hara JA, Dunn JF, and Swartz HM. Use of nitroxides for assessing perfusion, oxygenation, and viability of tissues: in vivo EPR and MRI studies. *Magn Reson Med* 35: 97–106, 1996.

51. Gallez B, Neveu MA, Danhier P, and Jordan BF. Manipulation of tumor oxygenation and radiosensitivity through modification of cell respiration: a critical review of approaches and imaging biomarkers for therapeutic guidance. *Biochim Biophys Acta* 1858: 700–711, 2017.

52. Gerken JB, Pang YQ, Lauber MB, and Stahl SS. Structural effects on the pH-dependent redox properties of organic nitroxyls: pourbaix diagrams for TEMPO, ABNO, and three TEMPO analogs. *J Org Chem* 83: 7323–7330, 2018.

53. Giotta GJ and Wang HH. Reduction of nitroxide free radicals by biological materials. *Biochem Biophys Res Commun* 46: 1576–1580, 1972.

54. Goda F, Bacic G, O'Hara JA, Gallez B, Swartz HM, and Dunn JF. The relationship between partial pressure of oxygen and perfusion in two murine tumors after X-ray irradiation: a combined gadopentetate dimeglumine dynamic magnetic resonance imaging and in vivo electron paramagnetic resonance oximetry study. *Cancer Res* 56: 3344–3349, 1996.

55. Goldstein S, Merenyi G, Russo A, and Samuni A. The role of oxoammonium cation in the SOD-mimic activity of cyclic nitroxides. *J Am Chem Soc* 125: 789–795, 2003.

56. Goldstein S and Samuni A. Kinetics and mechanism of peroxyl radical reactions with nitroxides. *J Phys Chem A* 111: 1066–1072, 2007.

57. Goldstein S, Samuni A, and Merenyi G. Kinetics of the reaction between nitroxide and thiyl radicals: nitroxides as antioxidants in the presence of thiols. *J Phys Chem A* 112: 8600–8605, 2008.

58. Goldstein S, Samuni A, and Russo A. Reaction of cyclic nitroxides with nitrogen dioxide: the intermediacy of the oxoammonium cations. *J Am Chem Soc* 125: 8364–8370, 2003.

59. Gomez-Mejiba SE and Ramirez DC. Trapping of DNA radicals with the nitrone spin trap 5,5-dimethyl-1-pyrroline N-oxide and genotoxic damage: recent advances using the immune-spin trapping technology. *Mutat Res* 782: 108283, 2019.

60. Gomez-Mejiba SE, Zhai Z, Akram H, Deterding LJ, Hensley K, Smith N, Towner RA, Tomer KB, Mason RP, and Ramirez DC. Immuno-spin trapping of protein and DNA radicals: ''tagging'' free radicals to locate and understand the redox process. *Free Radic Biol Med* 46: 853–865, 2009.

61. Gomi F, Utsumi H, Hamada A, and Matsuo M. Aging retards spin clearance from mouse brain and food restriction prevents its age-dependent retardation. *Life Sci* 52: 2027–2033, 1993.

62. Griesser M, Shah R, Van Kessel AT, Zilka O, Haidasz EA, and Pratt DA. The catalytic reaction of nitroxides with peroxyl radicals and its relevance to their cytoprotective properties. *J Am Chem Soc* 140: 3798–3808, 2018.

63. Griffiths HR, Gao D, and Pararasa C. Redox regulation in metabolic programming and inflammation. *Redox Biol* 12: 50–57, 2017.

64. Hahn SM, Sullivan FJ, DeLuca AM, Krishna CM, Wersto N, Venzon D, Russo A, and Mitchell JB. Evaluation of tempol radioprotection in a murine tumor model. *Free Radic Biol Med* 22: 1211–1216, 1997.

65. Halpern HJ, Jaffe DR, Nguyen TD, Haraf DJ, Spencer DP, Bowman MK, Weichselbaum RR, and Diamond AM. Measurement of bioreduction rates of cells with distinct responses to ionizing radiation and cisplatin. *Biochim Biophys Acta* 1093: 121–124, 1991.

66. Halpern HJ, Peric M, Yu C, Barth ED, and Chandramouli GVR. In vivo spin-label murine pharmacodynamics using low-frequency electron paramagnetic resonance imaging. *Biophys J* 71: 403–409, 1996.

67. Halpern HJ, Yu C, Barth E, Peric M, and Rosen GM. In situ detection, by spin trapping, of hydroxyl radical markers produced from ionizing radiation in the tumor of a living mouse. *Proc Natl Acad Sci U S A* 92: 796–800, 1995.

68. Han J-Y, Takeshita K, and Utsumi H. Noninvasive detection of hydroxyl radical generation in lung by diesel exhaust particles. *Free Radic Biol Med* 30: 516–525, 2001.

69. He G, Kutala VK, Kuppusamy P, and Zweier JL. In vivo measurement and mapping of skin redox stress induced by ultraviolet light exposure. *Free Radic Biol Med* 36: 665–672, 2004.

70. He G, Samouilov A, Kuppusamy P, and Zweier JL. In vivo EPR imaging of the distribution and metabolism of nitroxide radicals in human skin. *J Magn Reson* 148: 155–164, 2001.

71. Herrling T, Fuchs J, Rehberg J, and Groth N. UV-induced free radicals in the skin detected by ESR spectroscopy and imaging using nitroxides. *Free Radic Biol Med* 35: 59–67, 2003.

72. Herrling T, Jung K, and Fuchs J. Measurements of UV-generated free radicals/reactive oxygen species (ROS) in skin. *Spectrochim Acta A* 63: 840–845, 2006.

73. Hirayama A, Nagase S, Ueda A, Oteki T, Takada K, Obara M, Inoue M, Yoh K, Hirayama K, and Koyama A. In vivo imaging of oxidative stress in ischemia-reperfusion renal injury using electron paramagnetic resonance. *Am J Physiol Renal Physiol* 288: F597–F603, 2005.

74. Hirayama A, Ueda A, Oteki T, Nagase S, Aoyagi K, and Koyama A. In vivo imaging of renal redox status during azelnidipine treatment. *Hypertens Res* 31: 1643–1650, 2008.

75. Hirayama A, Yoh K, Nagase S, Ueda A, Itoh K, Morito N, Hirayama K, Takahashi S, Yamamoto M, and Koyama A. EPR imaging of reducing activity in Nrf2 transcriptional factor-deficient mice. *Free Radic Biol Med* 34: 1236–1242, 2003.

76. Hogston JL, Namazian M, Bottle SE, and Coote ML. One-electron oxidation and reduction potentials of nitroxide antioxidants: a theoretical study. *J Phys Chem A* 111: 13595–13605, 2007.

77. Hyodo F, Chuang K-H, Goloshevsky AG, Sulima A, Griffiths GL, Mitchell JB, Koretsky AP, and Krishna MC. Brain redox imaging using blood-brain barrier-permeable nitroxide MRI contrast agent. *J Cereb Blood Flow Metab* 28: 1165–1174, 2008.

78. Hyodo F, Davis RM, Hyodo E, Matsumoto S, Krishna MC, and Mitchell JB. The relationship between tissue oxygenation and redox status using magnetic resonance imaging. *Int J Oncol* 41: 2103–2109, 2012.

79. Hyodo F, Matsumoto K, Matsumoto A, Mitchel JB, and Krishna MC. Probing the intracellular redox status of tumors with magnetic resonance imaging and redox-sensitive contrast agents. *Cancer Res* 66: 9921–9928, 2006.

80. Hyodo F, Yasukawa K, Yamada K, and Utsumi H. Spatially resolved time-course studies of free radical reactions with an EPRI/MRI fusion technique. *Magn Reson Med* 56: 938–943, 2006.

81. Ilangovan G, Li H, Zweier JL, Krishna MC, Mitchell JB, and Kuppusamy P. In vivo measurement of regional oxygenation and imaging of redox status in RIF-1 murine tumor: effect of carbogen-breathing. *Magn Reson Med* 48: 723–730, 2002.

82. Isenberg JS, Hyodo F, Matsumoto K, Romeo MJ, Abu-Asab M, Tsokos M, Kuppusamy P, Wink DA, Krishna MC, and Roberts DD. Thrombospondin-1 limits ischemic tissue survival by inhibiting nitric oxide-mediated vascular smooth muscle relaxation. *Blood* 109:1945–1952, 2007.

83. Ivanova D, Bakalova R, Lazarova D, Gadjeva V, and Zhelev Z. The impact of reactive oxygen species on anticancer therapeutic strategies. *Adv Clin Exp Med* 22: 899–908, 2013.

84. Jiang J, Stoyanovsky DA, Belikova NA, Tyurina YY, Zhao Q, Tungekar MA, Kapralova V, Huang Z, Mintz AH, Greenberger JS, and Kagan VE. A mitochondrial-targeted triphenylphosphonium-conjugated nitroxide functions as a radioprotector/mitigator. *Radiat Res* 172: 706–717, 2009.

85. Jurkiewicz BA and Buettner GR. Ultraviolet light-induced free radical formation in skin: an electron paramagnetic resonance study. *Photochem Photobiol* 59: 1–4, 1994.

86. Jurkiewicz BA and Buettner GR. EPR detection of free radicals in UV-irradiated skin: mouse versus human. *Photochem Photobiol* 64: 918–922, 1996.

87. Karković Marković A, Jakobušić Brala C, Pilepić V, and Uršić S. Kinetic isotope effects and hydrogen tunnelling in PCET oxidations of ascorbate: new insights into aqueous chemistry? *Molecules* 25: 1443, 2020.

88. Karunakaran U and Park KG. A systematic review of oxidative stress and safety of antioxidants in diabetes: focus on islets and their defense. *Diabetes Metab J* 37: 106–112, 2013.

89. Kato Y, Shimizu Y, Yijing L, Unoura K, Utsumi H, and Ogata T. Reversible half-wave potentials of reduction processes on nitroxide radicals. *Electrochim Acta* 40: 2799–2802, 1995.

90. Keshari KR, Kurhanewicz J, Bok R, Larson PE, Vigneron DB, and Wilson DM. Hyperpolarized ^{13}C dehydroascorbate as an endogenous redox sensor for *in vivo* metabolic imaging. *Proc Natl Acad Sci U S A* 108: 18606–18611, 2011.

91. Keshari KR, Sai V, Wang ZJ, Vanbrocklin HF, Kurhanewicz J, and Wilson DM. Hyperpolarized [1–^{13}C]-dehydroascorbate MR spectroscopy in a murine model of prostate cancer: comparison with ^{18}F-FDG PET. *J Nucl Med* 54: 922–928, 2013.

92. Ketteler M, Wanner C, Metzger T, Bongartz P, Westenfeld R, Gladziwa U, Schurgers LJ, Vermeer C, Jahnen-Dechent W, and Floege J. Deficiencies of

calcium-regulatory proteins in dialysis patients: a novel concept of cardiovascular calcification in uremia. *Kidney Int Suppl* 84: S84–S87, 2003.

93. Keyse SM (Ed). *Stress Response: Methods and Protocols.* NJ: Humana Press, 2000.

94. Khan N and Swartz H. Measurements in vivo of parameters pertinent to ROS/RNS using EPR spectroscopy. *Mol Cell Biochem* 234–235: 341–357, 2002.

95. Khan N, Williams BB, and Swartz HM. Clinical applications of in vivo EPR: rationale and initial results. *Appl Magn Reson* 30: 185–199, 2006.

96. Kobayashi HP, Watanabe T, Oowada S, Hirayama A, Nagase S, Kamibayashi M, and Otsubo T. Effect of CV159-Ca^{2+}/calmodulin blockade on redox status hepatic ischemia-reperfusion injury in mice evaluated by a newly developed in vivo EPR imaging technique. *J Surg Res* 147: 41–49, 2008.

97. Koritzinsky M and Wouters BG. The role of ROS and autophagy in mediating the tolerance of tumor cells to cycling hypoxia. *Semin Radiol Oncol* 23: 252–261, 2013.

98. Kozlov AV, Szalay L, Umar F, Kropik K, Staniek K, Niedermuller H, Bahrami S, and Nohl H. Skeletalmuscles, heart, and lung are the main sources of oxygen radicals in old rats. *Biochim Biophys Acta* 1740: 382–389, 2005.

99. Krishna MC, Devasahayam N, Cook JA, Subramanian S, Kuppusamy P, and Mitchell JB. Electron paramagnetic resonance for small animal imaging applications. *ILAR J* 42: 209–218, 2001.

100. Kumar A, Ganini D, and Mason RP. Role of cytochrome c in alpha-synuclein radical formation: implications of alpha-synuclein in neuronal death in Maneb- and paraquat-induced model of Parkinson's disease. *Mol Neurodegener* 11: 70, 2016.

101. Kuppusamy P, Afeworki M, Shankar RA, Coffin D, Krishna MC, Hahn SM, Mitchell JB, and Zweier JL. In vivo electron paramagnetic resonance imaging of tumor heterogeneity and oxygenation in a murine model. *Cancer Res* 58: 1562–1568, 1998.

102. Kuppusamy P, Li H, Ilangovan G, Cardounel AJ, Zweier JL, Yamada K, Krishna MC, and Mitchell JB. Noninvasive imaging of tumor redox status and its modification by tissue glutathione levels. *Cancer Res* 62: 307–312, 2002.

103. Lazarova D, Shibata S, Ishii I, Zlateva G, Zhelev Z, Aoki I, Higashi T, and Bakalova R. Nitroxide-enhanced MRI of kidney dysfunction in vivo based on redox-imbalance and oxidative stress. *Gen Physiol Biophys* 38: 191–204, 2019.

104. Leonard SS, Mowrey K, Pack D, Shi X, Castranova V, Kuppusamy P, and Vallyathan V. In vivo bioassays of acute asbestosis and its correlation with ESR spectroscopy and imaging in redox status. *Mol Cell Biochem* 234–235: 369–377, 2002.

105. Likhtenshtein GI. Nitroxide chemical reactions. In: *Nitroxides*. Springer Series in Materials Science, Vol. 292. pp. 35–69. Cham: Springer, 2020.

106. Likhtenshtein GI, Yamauchi J, Nakatsuji S, Smirnov AI, and Tamura R (Eds). *Nitroxides: Applications in Chemistry, Biomedicine, and Material Science.* Weinheim: Wiley-VCH, 2008.

107. Liu Y, Li Q, Zhou L, Xie N, Nice EC, Zhang H, Huang C, and Lei Y. Cancer drug resistance: redox resetting renders a way. *Oncotarget* 7: 42740–42761, 2016.

108. Luzhkov VB. Treatment of the conformational contribution in quantum mechanical calculations of the redox potentials of nitroxyl radicals. *Russ J Phys Chem A* 94: 908–913, 2020.

109. Mader K, Bacic G, and Swartz HM. *In vivo* detection of anthralin-derived free radicals in the skin of hairless mice by low-frequency electron paramagnetic resonance spectroscopy. *J Investig Dermatol* 104: 514–517, 1995.

110. Malek M and Nematbakhsh M. Renal ischemia/reperfusion injury; from pathophysiology to treatment. *J Renal Inj Prev* 4: 20–27, 2015.

111. Manda S, Nakanishi I, Ohkubo K, Kawashima T, Matsumoto K, Ozawa T, Fukuzumi S, Ikota N, and Anzai K. Effect of solvent polarity on the one-electron oxidation of cyclic nitroxyl radicals. *Chem Lett* 36: 914–915, 2007.

112. Manda S, Nakanishi I, Ohkubo K, Yakumaru H, Matsumoto K, Ozawa T, Ikota N, Fukuzumi S, and Anzai K. Nitroxyl radicals: electrochemical redox behaviour and structure–activity relationships. *Org Biomol Chem* 5: 3951–3955, 2007.

113. Mannaerts D, Faes E, Gielis J, Briede J, Cos P, Van Craenenbroeck E, Gyselaers W, Cornette J, Spaanderman M, and Jacquemyn Y. Oxidative stress in maternal serum as andothelial dysfunction marker in preeclampsia, an EPR pilot study. *J Matern Fetal Neonatal Med* 29: 3, 2016.

114. Marchesi E, Rota C, Fann YC, Chignell CF, and Mason RP. Photoreduction of the fluorescent dye dichlorofluorescein: a spin trapping and direct electron spin resonance study with implications for oxidative stress measurements. *Free Radic Biol Med* 26: 148–161, 1999.

115. Mason RP. Using anti-5,5-dimethyl-1-pyrroline-*N*-oxide (anti-DMPO) to detect protein radicals in time and space with immuno-spin trapping. *Free Radic Biol Med* 36: 1214–1223, 2004.

116. Mathew S, Lund RJ, Strebeck F, Tustison KS, Geurs T, and Hruska KA. Reversal of the adynamic bone disorder and decreased vascular calcification in chronic kidney disease by sevelamer carbonate therapy. *J Am Soc Nephrol* 8: 122–123, 2007.

117. Matsumoto K. Utility decay rates of T_1-weighted magnetic resonance imaging contrast based on redox-sensitive paramagnetic nitroxyl contrast agents. *Biol Pharm Bull* 32: 711–716, 2009.

118. Matsumoto K, Hyodo F, Anzai K, Utsumi H, Mitchell JB, and Krishna MC. Brain redox imaging. *Methods Mol Biol* 711: 397–419, 2011.

119. Matsumoto K, Hyodo F, Matsumoto A, Koretsky AP, Sowers AL, Mitchell JB, and Krishna MC. High resolution mapping of tumor redox status by magnetic resonance imaging using nitroxides as redox-sensitive contrast agents. *Clin Cacer Res* 12: 2455–2462, 2006.

120. Matsumoto S, Koshiishi I, Inoguchi T, Nawata H, and Utsumi H. Confirmation of superoxide generation via xanthine oxidase in streptozotocin-induced diabetic mice. *Free Radic Res* 37: 767–772, 2003.

121. Matsumoto S, Mori N, Tsuchihashi N, Ogata T, Lin Y, Yokoyama H, and Ishida S. Enhancement of nitroxide-reducing activity in rats after chronic administration of vitamin E, vitamin C, and idebenone examined by an in vivo electron spin resonance technique. *Magn Reson Med* 40: 330–333, 1998.

122. Matsumoto K, Nyui M, Ueno M, Ogawa Y, and Nakanishi I. A quantitative analysis of carbon-ion beam-induced reactive oxygen species and redox reactions. *J Clin Biochem Nutr* 65: 1–7, 2019.

123. Matsumoto K, Subramanian S, Murugesan R, Mitchell JB, and Krishna MC. Spatially resolved biological information from in vivo EPRI, OMRI, and MRI. *Antioxid Redox Signal* 9: 1125–1141, 2007.

124. Matsumoto K, Yakumaru H, Narazaki M, Nakagawa H, Anzai K, Ikehira H, and Ikota N. Modification of nitroxyl contrast agents with multiple spins and their proton T_1 relaxivity. *Magn Reson Imaging* 26: 117–121, 2008.

125. Matsumoto K, Yamasaki T, Nakamura M, Ishikawa J, Ueno M, Nakanishi I, Sekita A, Ozawa Y, Kamada T, Aoki I, and Yamada K. Brain contrasting ability of blood-brain-barrier-permeable nitroxyl contrast agents for magnetic resonance RedOx imaging. *Magn Reson Med* 76: 935–945, 2016.

126. Metz JM, Smith D, Mick R, Lustig R, Mitchell J, Cherakuri M, Glatstein E, and Hahn SM. A phase I study of topical Tempol for the prevention of alopecia induced by whole brain radiotherapy. *Clin Cancer Res* 10: 6411–6417, 2004.

127. Mikuni T, He G, Petryakov S, Fallouh MM, Deng Y, Ishihara R, Kuppusamy P, Tatsuta M, and Zweier JL. In vivo detection of gastric cancer in rats by electron paramagnetic resonance imaging. *Cancer Res* 64: 6495–6502, 2004.

128. Milman Z, Axelrod JH, Heyman SN, Nachmansson N, and Abramovich R. Assessment with unenhanced MRI techniques of renal morphology and hemodynamic changes during acute kidney injury and chronic kidney disease in mice. *Am J Nephrol* 39: 268–278, 2014.

129. Mitchell JB, Russo A, Kuppusamy P, and Krishna MC. Radiation, radicals, and images. *Ann N Y Acad Sci* 899: 28–43, 2000.

130. Mittal M, Siddiqui MR, Tran K, Reddy SP, and Malik AB. Reactive oxygen species in inflammation and tissue injury. *Antioxid Redox Signal* 20: 1126–1167, 2014.

131. Miura Y, Anzai K, Urano S, and Ozawa T. In vivo electron paramagnetic resonance studies on oxidative stress caused by X-irradiation in whole mice. *Free Radic Biol Med* 23: 533–540, 1997.

132. Miura Y, Utsumi H, Kashiwagi M, and Hamada A. Effects of oxygen on the membrane structure and the metabolism of lipophilic nitroxide in rat liver microsomes. *J Biochem* 108: 516–518, 1990.

133. Morris S, Sosnovsky G, Hui B, Huber CO, Rao NU, and Swartz HM. Chemical and electrochemical reduction rates of cyclic nitroxides (nitroxyls). *J Pharm Sci* 80: 149–152, 1991.

134. Mucaj V, Shay JES, and Simon MC. Effects of hypoxia and HIFs on cancer metabolism. *Int J Hematol* 95: 464–470, 2012.

135. Nakamura M, Shibata S, Yamasaki T, Ueno M, Nakanishi I, Matsumoto K, Kamada T, Yamada K, and Aoki I. Feasibility of magnetic resonance redox imaging at low magnetic field: comparison at 1 T and 7 T. *Am J Transl Res* 9: 4481–4491, 2017.

136. Nakamura M, Yamasaki T, Ueno M, Shibata S, Ozawa Y, Kamada T, Nakanishi I, Yamada K, Aoki I, and Matsumoto K. Radiation-induced redox alteration in the mouse brain. *Free Radic Biol Med* 143: 412–421, 2019.

137. Nakanishi I, Kawaguchi K, Ohkubo K, Kawashima T, Manda S, Kanazawa H, Takeshita K, Anzai K, Ozawa T, Fukuzumi S, and Ikota N. Scandium ion-accelerated scavenging reaction of cumylperoxyl radical by a cyclic nitroxyl radical via electron transfer. *Chem Lett* 36: 378–379, 2017.

138. Nakanishi I, Shoji Y, Ohkubo K, Ozawa T, Matsumoto K, and Fukuzumi S. A large kinetic isotope effect in the reaction of ascorbic acid with 2-phenyl-4,4,5,5-tetramethylimazolione-1-oxide (PTIO•) in aqueous buffer solutions. *Chem Commun* 56: 11505–11507, 2020.

139. Nguyen HV, Detappe A, Gallagher NM, Zhang H, Harvey P, Yan C, Mathieu C, Golder MR, Jiang Y, Ottaviani MF, Jasanoff A, Rajca A, Ghobrial I, Ghoroghchian PP, and Johnson JA. Triply loaded nitroxide brush-arm star polymers enable metal-free millimetric tumor detection by magnetic resonance imaging. *ACS Nano* 12: 11343–11354, 2018.

140. Nishino N, Yasui H, and Sakurai H. In vivo L-band ESR and quantitative pharmacokinetic analysis of stable spin probes in rats and mice. *Free Radic Res* 31: 35–51, 1999.

141. Novo E and Parola M. Redox mechanisms in hepatic chronic wound healing and fibrogenesis. *Fibrogenesis Tissue Repair* 1: 5, 2008.

142. Nutting JE, Rafiee M, and Stahl SS. Tetramethylpiperidine *N*-oxyl (TEMPO), phthalimide *N*-oxyl (PINO), and related *N*-oxyl species: electrochemical properties and their use in electrocatalytic reactions. *Chem Rev* 118: 4834–4885, 2018.

143. Pervaiz S and Clement MV. Superoxide anion: oncogenic reactive oxygen species? *Int J Biochem Cell Biol* 39: 1297–1304, 2007.

144. Phumala N, Ide T, and Utsumi H. Noninvasive evaluation of in vivo free radical reactions catalyzed by iron using in vivo ESR spectroscopy. *Free Radic Biol Med* 26: 1209–1217, 1999.

145. Prowle JR, Molan MP, Hornsey E, and Bellomo R. Cine phase-contrast MRI for the measurement of renal blood flow. *Contrib Nephrol* 165: 329–336, 2010.

146. Ramirez DC, Chen YR, and Mason RP. Immunochemical detection of hemoglobin-derived radicals formed by reaction with hydrogen peroxide: involvement of a protein-tyrosyl radical. *Free Radic Biol Med* 34: 830–839, 2003.

147. Redler G, Barth ED, Bauer KS, Kao JPY, Rosen GM, and Halpern HJ. In vivo electron paramagnetic resonance imaging of differential tumor targeting using cis-3,4-di(acetoxymethoxycarbonyl)-2,2,5,5-tetramethyl-1-pyrrolidinyloxyl. *Magn Reson Med* 71: 1650–1656, 2014.

148. Rodriguez-Lara SQ, Cardona-Munoz EG, Ramirez-Lizardo EJ, Totsuka-Sutto SE, Castillo-Romero A, Garcia-Cobian TA, and Garcia-Benavides L. Alternative interventions to prevent oxidative damage following ischemia/reperfusion. *Oxid Med Cell Longev* 2016: 7190943, 2016.

149. Roman-Pintos LM, Villegas-Rivera G, Rodriguez-Carrizalez AD, Miranda-Diaz AG, and Cardona-Munoz EG. Diabetic polyneuropathy in type 2 diabetes mellitus: inflammation, oxidative stress, and mitochondrial function. *J Diabetes Res* 2016: 3425617, 2016.

150. Roshchupkina GI, Bobko AA, Bratasz A, Reznikov VA, Kuppusamy P, and Khramtsov VV. In vivo EPR measurement of glutathione in tumor-bearing mice using improved disulfide biradical probe. *Free Radic Biol Med* 45: 312–320, 2008.

151. Rovcanin B, Medic B, Kocic G, Cebovic T, Ristic M, and Prostran M. Molecular dissection of renal ischemia-reperfusion: oxidative stress and cellular events. *Curr Med Chem* 23: 1965–1980, 2016.

152. Ruiz MC, Medina A, Moreno JM, Gomez I, Ruiz N, Bueno P, Asensio C, and Osuna A. Relationship between oxidative stress parameters and atherosclerotic signs in the carotid artery of stable renal transplant patients. *Transplant Proc* 37: 3796–3798, 2005.

153. Sajenko I, Pilepić V, Jakobušić Brala C, and Uršić S. Solvent dependence of the kinetic isotope effect in the reaction of ascorbate with the 2,2,6,6-tetramethylpiperidine-1-pxyl radical: tunneling in a small molecule reaction. *J Phys Chem A* 114: 3423–3430, 2010.

154. Samouilov A, Caia GL, Kesselring E, Petryakov S, Wasowicz T, and Zweier JL. Development of a hybrid EPR/NMR coimaging system. *Magn Reson Med* 58: 156–166, 2007.

155. Samuni A, Goldstein S., Russo A, Mitchell JB, Krishna MC, and Neta P. Kinetics and mechanism of hydroxyl radical and OH-adduct radical reactions with nitroxides and with their hydroxylamines. *J Am Chem Soc* 124: 8719–8724, 2002.

156. Sano H, Matsumoto K, and Utsumi H. Synthesis and imaging of blood-brain-barrier permeable nitroxyl-probes for free radical reactions in brain of living mice. *Biochem Mol Biol Int* 42: 641–647, 1997.

157. Sano H, Naruse M, Matsumoto K, Oi T, and Utsumi H. A new nitroxyl-probe with high retention in the brain and its application for brain imaging. *Free Radic Biol Med* 28: 959–969, 2000.

158. Sano T, Umeda F, Hashimoto T, Nawata H, and Utsumi H. Oxidative stress measurement by in vivo electron spin resonance spectroscopy in rats with streptozotocin-induced diabetes. *Diabetologia* 41: 1355–1360, 1998.

159. Sato-Akaba H, Fujii H, and Hirata H. Development and testing of a CW-EPR apparatus for imaging of short-lifetime nitroxyl radicals in mouse head. *J Magn Reson* 193: 191–198, 2008.

160. Sen CK. Wound healing essentials: let there be oxygen. *Wound Repair Regen* 17: 1–18, 2009.

161. Sonta T, Inoguchi T, Matsumoto S, Yasukawa K, Inuo M, Tsubouchi H, Sonoda N, Kobayashi K, Utsumi H, and Nawata H. In vivo imaging of oxidative stress in the kidney of diabetic mice and its normalization by angiotensin II type 1 receptor blocker. *Biochem Biophys Res Commun* 330: 415–422, 2005.

162. Sonta T, Inoguchi T, Tsubouchi H, Sekiguchi N, Kobayashi K, Matsumoto S, Utsumi H, and Nawata H. Evidence for contribution of vascular NAD(P)H oxidase to increased oxidative stress in animal models of diabetes and obesity. *Free Radic Biol Med* 37: 115–123, 2004.

163. Soule BP, Hyodo F, Matsumoto K, Simone NL, Cook JA, Krishna MC, and Mitchell JB. The chemistry and biology of nitroxide compounds. *Free Radic Biol Med* 42: 1632–1650, 2007.

164. Soule BP, Hyodo F, Matsumoto K, Simone NL, Cook JA, Krishna MC, and Mitchell JB. Therapeutic and clinical applications of nitroxide compounds. *Antioxid Redox Signal* 9: 1731–1743, 2007.

165. Stokman G, Kors L, Bakker PJ, Rampanelli E, Claessen N, Teske GJD, Butter L, van Andel H, van den Bergh Weerman MA, Larsen PWB, Dessing MC, Zuurbier CJ, Girardin SE, Florquin S, and Leemans JC. NLRX1 dampens oxidative stress and apoptosis in tissue injury via control of mitochondrial activity. *J Exp Med* 214: 2405–2420, 2017.

166. Subramanian S, Matsumoto K, Mitchell JB, and Krishna MC. Radio frequency continuous-wave and time-domain EPR imaging and Overhauser-enhanced magnetic resonance imaging of small animals: instrumental developments and comparison of relative merits for functional imaging. *NMR Biomed* 17: 263–294, 2004.

167. Takeshita K, Chi C, Hirata H, Ono M, and Ozawa T. In vivo generation of free radicals in the skin of live mice under ultraviolet light, measured by L-band EPR spectroscopy. *Free Radic Biol Med* 40: 876–885, 2006.

168. Takeshita K, Kawaguchi K, Fujii-Aikawa K, Ueno M, Okazaki S, Ono M, Krishna MC, Kuppusamy P, Ozawa T, and Ikota N. Heterogeneity of regional redox status and relation of the redox status to oxygenation in a tumor model, evaluated using electron paramagnetic resonance imaging. *Cancer Res* 70: 4133–4140, 2010.

169. Takeshita K and Ozawa T. Recent progress in in vivo ESR spectroscopy. *J Radiat Res* 45: 373–384, 2004.

170. Takeshita K, Takajo T, Hirata H, Ono M, and Utsumi H. In vivo oxygen radical generation in the skin of the protoporphyria model mouse with visible light exposure: an L-band ESR study. *J Investig Dermatol* 122: 1463–1470, 2004.

171. Togashi H, Matsuo T, Shinzawa H, Takeda Y, Shao L, Oikawa K, Kamada H, and Takahashi T. Ex vivo measurement of tissue distribution of a nitroxide radical after intravenous injection and its in vivo imaging using a rapid scan ESR-CT system. *Magn Reson Imaging* 18: 151–156, 2000.

172. Togashi H, Shinzawa H, Ogata T, Matsuo T, Ohno S, Saito K, Yamada N, Yokoyama H, Noda H, Oikawa K, Kamada H, and Takahashi T. Spatiotemporal measurement of free radical elimination in the abdomen using an in vivo ESR/CT imaging system. *Free Radic Biol Med* 25: 1–8, 1998.

173. Tomizawa A, Hadjidekov G, Ishii I, Bakalova R, Zhelev Z, Aoki I, Saga T, and Kitada M. Nitroxide derivatives for imaging of hypercholesterolemia-induced kidney dysfunction and assessing the effectiveness of antilipidemic drugs. *Mol Pharm* 8: 1962–1969, 2011.

174. Trachootham D, Lu W, Ogasawara MA, Del Valle NR, and Huang P. Redox regulation in cell survival. *Antioxid Redox Signal* 10: 1343–1374, 2008.

175. Trachootham D, Zhang H, Zhang W, Feng L, Du M, Zhou Z, Pelicano H, Plunkett W, Wierda WG, Keating MJ, and Huang P. Effective elimination of fludarabine-resistant CLL cells by PEITC through a redox-mediated mechanism. *Blood* 112: 1912–1922, 2008.

176. Tsubouchi H, Inoguchi T, Sonta T, Sato N, Sekiguchi N, Kobayashi K, Sumimoto H, Utsumi H, and Nawata H. Statin attenuates high glucose-induced and diabetes-induced oxidative stress in vitro and in vivo evaluated by electron spin resonance measurement. *Free Radic Biol Med* 39: 444–452, 2005.

177. Tsunaga M, Iwakura C, and Tamura H. Electrode reactions of nitroxide radicals at platinum in acetonitrile. *Electrochim Acta* 18: 241–245, 1973.

178. Ueda Y, Yokoyama H, Nakajima A, Ohya-Nishiguchi H, and Kamada H. In vivo electron spin resonance spectroscopy on signal decay of intrastriatal nitroxide radical after acute administration of haloperidol in rats. *Brain Res Bull* 51: 313–317, 2000.

179. Utsumi H, Sano H, Naruse M, Matsumoto K, Ichikawa K, and Oi T. Nitroxyl probes for brain research and their application to brain imaging. *Methods Enzymol* 352: 494–506, 2002.

180. Utsumi H and Yamada K. In vivo electron spin resonance-computed tomography/nitroxyl probe technique for non-invasive analysis of oxidative injuries. *Arch Biochem Biophys* 416: 1–8, 2003.

181. Vanea E, Charlier N, DeWever J, Dinguizli M, Feron O, Baurain J-F, and Gallez B. Molecular electron paramagnetic resonance imaging of melanin in melanomas: a proof-of-concept. *NMR Biomed* 21: 296–300, 2008.

182. Vila M and Przedborski S. Targeting programmed cell death in neurodegenerative diseases. *Nat Rev Neurosci* 4: 1–11, 2003.

183. Yamada K, Kuppusamy P, English S, Yoo J, Irie A, Subramanian S, Mitchell JB, and Krishna MC. Feasibility and assessment of non-invasive in vivo redox status using electron paramagnetic resonance imaging. *Acta Radiol* 43: 433–440, 2002.

184. Yamada K, Yamamiya I, and Utsumi H. In vivo detection of free radicals induced by diethylnitrosamine in rat liver tissue. *Free Radic Biol Med* 40: 2040–2046, 2006.

185. Yamasaki T, Mito F, Ito Y, Pandian S, Kinoshita Y, Nakano K, Murugesan R, Sakai K, Utsumi H, and Yamada K. Structure–reactivity relationship of piperidine nitroxide: electrochemical, ESR and computational studies. *J Org Chem* 76: 435–440, 2011.

186. Yasukawa K, Shigemi R, Kanbe T, Mutsumoto Y, Oda F, Ichikawa K, Yamada KI, Tun X, and Utsumi H. In vivo imaging of the intra- and extracellular redox status in rat stomach with indomethacin-induced gastric ulcers using Overhauser-enhanced magnetic resonance imaging. *Antioxid Redox Signal* 30: 1147–1161, 2019.

187. Yokoyama H, Ishida S-I, and Ogata T. In vivo temporal EPR study using a region-selected intensity determination method to estimate cerebral reducing ability in rats treated with olanzapine. *Magn Reson Imaging* 28: 898–902, 2010.

188. Yokoyama H, Itoh O, Aoyama M, Obara H, Ohya H, and Kamada H. In vivo EPR imaging by using an acyl-protected hydroxylamine to analyse intracerebral oxidative stress in rats after epileptic seizures. *Magn Reson Imaging* 18: 875–879, 2000.

189. Yokoyama H, Itoh O, Ohya-Nishiguchi H, and Kamada H. Reducing ability of the striatum and cerebral cortex in rats following acute administration of risperidone or haloperidol: an estimation by in vivo electron paramagnetic resonance imaging. *Neurochem Res* 27: 243–248, 2002.

190. Yokoyama H, Lin Y, Itoh O, Ueda Y, Nakajima A, Ogata T, Sato T, Ohya-Nishiguchi H, and Kamada H. EPR imaging for in vivo analysis of the half-life of a nitroxide radical in the hippocampus and cerebral cortex of rats after epileptic seizures. *Free Radic Biol Med* 27: 442–448, 1999.

191. Yokoyama H, Morinobu S, and Ueda Y. EPRI to estimate the in vivo intracerebral reducing ability in adolescent rats subjected to neonatal isolation. *J Magn Reson Imaging* 23: 637–640, 2006.

192. Zarling JA, Brunt VE, Vallerga AK, Li W, Tao A, Zarling DA, and Minson CT. Nitroxide pharmaceutical development for age-related degeneration and disease. *Front Genet* 6: 325, 2015.

193. Zhang K, Noble BB, Mater AC, Monteiro MJ, Coote ML, and Jia Z. Effect of heteroatom and functionality substitution on the oxidation potential of cyclic nitroxide radicals: role of electrostatics in electrochemistry. *Phys Chem Chem Phys* 20: 2606–2614, 2018.

194. Zhelev Z, Aoki I, Gadjeva V, Nikolova B, Bakalova R, and Saga T. Tissue redox activity as a sensing platform for imaging of cancer based on nitroxide redox cycle. *Eur J Cancer* 49: 1467–1478, 2013.

195. Zhelev Z, Bakalova R, Aoki I, Lazarova D, and Saga T. Imaging of superoxide generation in the dopaminergic area of the brain in Parkinson's disease, using mito-TEMPO. *ACS Chem Neurosci* 4: 1439–1445, 2013.

196. Zhelev Z, Bakalova R, Aoki I, Matsumoto K, Gadjeva V, Anzai K, and Kanno I. Nitroxyl radicals as low toxic spin-labels for non-invasive magnetic resonance imaging of blood–brain barrier permeability for conventional therapeutics. *Chem Commun* 2009: 53–55, 2009.

197. Zhelev Z, Bakalova R, Gadjeva V, and Kanno I. Imaging of cancer by redox-mediated mechanism: a radical diagnostic approach. *Mol Biosyst* 6: 2386–2388, 2010.

198. Zhelev Z, Gadjeva V, Aoki I, Bakalova R, and Saga T. Cell-penetrating nitroxides as molecular sensors for imaging of cancer in vivo based on tissue redox activity. *Mol Biosyst* 8: 2733–2740, 2012.

199. Zhelev Z, Georgieva E, Lazarova D, Semkova S, Aoki I, Gulubova M, Higashi T, and Bakalova R. Redox imaging to distinguish cells with different proliferative index: superoxide, hydroperoxides and their ratio as potential biomarkers. *Oxid Med Cell Longev* 2019: 6373685, 2019.

200. Zuo L, Chen YR, Reyes LA, Lee HL, Chen CL, Villamena FA, and Zweier JL. The radical trap 5,5-dimethyl-1-pyrroline *N*-oxide exerts dose-dependent protection against myocardial ischemia-reperfusion injury through preservation of mitochondrial electron transport. *J Pharmacol Exp Ther* 329: 515–523, 2009.

Address correspondence to:
Dr. Ken-ichiro Matsumoto
Quantitative RedOx Sensing Group
Department of Radiation Regulatory Science Research
National Institute of Radiological Sciences
Quantum Life and Medical Science Directorate
National Institutes for Quantum
and Radiological Science and Technology
4-9-1 Anagawa, Inage-ku
Chiba-shi 263-8555
Chiba
Japan

E-mail: matsumoto.kenichiro@qst.go.jp

Abbreviations Used

•H = hydrogen radicals
•OH = hydroxyl radicals
23c = 4-(*N*-methylpiperidine)-2,2,5,5-tetramethylpyrroline-*N*-oxyl
2D = two dimensional
3D = three dimensional
AA = ascorbic acid
BBB = blood–brain barrier
carbamoyl-PROXYL = 3-carbamoyl-2,2,5,5-tetramethylpyrrolidine-*N*-oxyl
carboxy-PROXYL = 3-carboxy-2,2,5,5-tetramethylpyrrolidine-*N*-oxyl
CAT1 = 4-trimethylammonium-2,2,6,6-tetramethylpiperidine-*N*-oxyl
CCl_4 = carbon tetrachloride
CD = cholesterol diet
CW = continuous wave
CxP-Am = acetoxymethyl-2,2,5,5-tetramethylpyrrolidine-*N*-oxyl-3-carboxylate

Abbreviations Used (Cont.)

DMPO = 5,5-dimethyl-1-pyrroline-*N*-oxide

DNP = dynamic nuclear polarization

DT = dopamine transporter

EPR = electron paramagnetic resonance

EPRI = EPR imaging

FA = flip angle

FLASH = fast low angle shot

H_2O_2 = hydrogen peroxide

HM-PROXYL = 3-(hydroxymethyl)-1-oxy-2,2,5,5-tetramethylpyrrolidine

$HO_2{}^\bullet$ = hydroperoxyl radical

HRP = horseradish peroxidase

KA = kainic acid

KIE = kinetic isotope effects

LPS = lipopolysaccharides

MCP-H = hydroxylamine form of MC-PROXYL

MC-PROXYL = 3-methoxycarbonyl-2,2,5,5-tetramethylpyrrolidine-*N*-oxyl

mito-TEMPO = 2,2,6,6-tetramethyl-4[[2-(triphenylphosphonio)acetyl]amino]-1-piperidinyloxy

mito-TEMPO-H = hydroxylamine form of mito-TEMPO

MPP^+ = 1-methyl-4-phenylpyridinium

MPTP = 1-methyl-4-phenyl-1,2,3,6-tetrahydropyridine

MR = magnetic resonance

MRI = magnetic resonance imaging

ND = normal diet

O_2 = oxygen

$O_2{}^{\bullet-}$ = superoxide

OMRI = Overhauser-enhanced MRI

pO_2 = partial oxygen pressure

PP-H = hydroxylamine form of 4-phosphonooxy-TEMPO

ROI = region of interest

$ROO^\bullet$ = peroxyl radical

ROS = reactive oxygen species

Rot = rotenone

$RS^\bullet$ = thiyl radicals

SD = standard deviation

SG = salivary gland

SLENU = TEMPO-labeled nitrosourea

SNpc = substantia nigra pars compacta

TE = echo time

TEMPO = 2,2,6,6-tetramethylpiperidine-*N*-oxyl

$TEMPO^+$ = oxoammonium form of TEMPO

TEMPO-H = hydroxylamine form of TEMPO

TEMPOL = 4-hydroxy-2,2,6,6-tetramethylpiperidine-*N*-oxyl

TES = 4-[(3-carboxy-1-oxopropyl)amino]-2,2,6,6-tetramethyl-1-piperidinyloxy

TR = repetition time